VILNIUS UNIVERSITY

PHYSICS INSTITUTE OF CENTRE FOR PHYSICAL SCIENCES AND TECHNOLOGY

Povilas Keburis

BROADBAND DIELECTRIC SPECTROSCOPY OF LEAD-FREE FERROELECTRIC RELAXORS

Doctoral Dissertation

Physical Science, Physics (02 P)

Vilnius, 2011

The doctoral dissertation was prepared in Vilnius University in 2005-2010

Academic supervisor:

Prof. Dr. Habil. Jūras Banys (Vilnius University, Physical Science, Physics – 02P)

VILNIAUS UNIVERSITETAS

FIZINIŲ IR TECHNOLOGINIŲ MOKSLŲ CENTRO
FIZIKOS INSTITUTAS

Povilas Keburis

BEŠVINIŲ FEROELEKTRINIŲ RELAKSORIŲ PLAČIAJUOSTĖ DIELEKTRINĖ SPEKTROSKOPIJA

Daktaro disertacija

Fiziniai mokslai, fizika (02 P)

Vilnius, 2011

Disertacija rengta 2005-2010 metais Vilniaus universitete.

Mokslinis vadovas:

Prof. habil. dr. Jūras Banys (Vilniaus universitetas, fiziniai mokslai, fizika – 02P)

CONTENTS

INTRODUCTION

Ferroelectric fenomena have attracted considerable attention from the beginning of 20 th century, when American scientist of Czech origin J. Valasek discovered spontaneous electric polarization and it's electric hysterezis in Rochelle (or Seignette) salt [1]. Nowadays, relaxor ferroelectrics (*relaxors, RLs*) have gained significant attention due to their unusual physical behaviour and excellent dielectric and electromechanical properties. Lead-free ferroelectric relaxor ceramics have been intensively investigated in order to replace widely used PMN, PZT, PLZT and other lead-containing materials, according to the EU legislation restricting the use of hazardous substances in electrical and electronic equipment [2]. Dielectric measurements of relaxors are very important for both fundamental investigations and applications. However most of such investigations are performed only in narrow frequency range [3-9]. Often only the increase of temperature value, at which the dielectric permittivity has maximum, with increase of frequency, is analysed. As a rule, such investigations are based on various predefined formulas of distribution of relaxation times. Most popular predefined distribution of relaxation times is the Cole-Cole function [10-13], however this model is good enough only for narrowband dielectric data of relaxors. On the other hand, two or more Cole-Cole functions describe dielectric dispersion better in relaxors; however a further drawback of such an approach is the inherent difficulty of separating processes with comparable relaxation times. Other predefined distribution functions: Davidson-Cole [14], Havriliak-Negami [15], Joncher, Kolraush-Wiliams-Watts and Curie-von Schweidler [16] also frequently are used for analysis of dielectric data of relaxors, however such analysis can not explain dynamics of polar nanoregions.

Broadband dielectric spectroscopy from Hz to GHz region is needed for investigation of very wide dielectric relaxation in relaxors. We can predicate that dielectric dispersion of bulk relaxors at higher temperature (near and below T_B) is rather unknown, because the dielectric dispersion at higher

temperatures is revealed mainly in microwave and THz region. On the other hand, in literature there are many speculations about relaxor dynamics based on hypothesis about the dielectric dispersion between several GHz and several hundred GHz. The authors of [17] discovered two dielectric dispersions in relaxors, one from low frequencies to 1.8 GHz and another between 1.8 GHz and several hundred GHz, however they have no data between 1.8 GHz and 100 GHz. Dielectric and piezoelectric studies of solid solutions of relaxor ferroelectrics like $Pb(Mg_{1/3}Nb_{2/3})O_3$ (PMN) and $Pb(Sc_{1/2}Nb_{1/2})O_3$ (PSN) with normal ferroelectric $PbTiO_3$ revealed giant piezoelectricity (one order of magnitude larger than in the best classical ferroelectrics like $PbZr_{1-x}Ti_xO_3$) for compositions near morphotropic phase boundary [18]. The paper of Park and Shrout [18] turned the attention of many physicists to the study of solid solutions of relaxor ferroelectrics with ferroelectrics. Monoclinic phase was observed on the morphotrophic phase boundary between the tetragonal and rhombohedral phases [19] and it was proposed that the easy rotation of polarization in the monoclinic phase is responsible for the giant piezoelectric coefficient in these systems [20]. Appearance of polar nanoregions (PNRs) and their dynamics in lead-based perovskite relaxors have been thoroughly investigated by a wide range dielectric spectroscopy [21-23]. However, for lead-free relaxors no complete data on their dielectric spectra were reported and analysed so far.

The aim of the work

The aim of the the work was to investigate the collective phenomena in disordered ferroelectrics.

The tasks of the dissertation:

1. Investigation of lead-free materials in broad temperature and frequency range.
2. Investigation of ferroelectric phase transition dynamics in isovalently and heterovalently dopped $BaTiO_3$.

3. Dielectric measurements of xBBT-(1-x)SBT solid solutions in order to confirm the crossover from ferroelectric to relaxor state.
4. Piezoresponse Force Microscopy (PFM) and dielectric measurements and investigation of dynamics of polar nanoregions in $BaBi_2Nb_2O_9$ ceramics.

Scientific novelty

1. For the first time the dielectric response of (1-*x*)BT-*x*LMT, xBBT-(1-x)SBT, $BaTi_{1-x}Sn_xO_3$ and $BaBi_2Nb_2O_9$ ceramics in microwave frequency was measured.
2. The function of the distribution of the relaxation times of above mentioned materials was calculated from the dielectric spectra for the first time.
3. Polar nanoregions sized about 50 nm of BBN ceramics were observed using PFM method.
4. The relaxation time distribution function of BBN ceramics was fitted with the formalism developed for the dipolar glasses.

The statements presented for the defense

1. Dielectric dispersion in the lead-free ferroelectric ceramics is caused by polar nanoregions (PNR's).
2. The influence of polar nanoregions to the distribution of relaxation times gives broadening to the long relaxational times according to Vogel-Fulcher law.
3. Even small substitution of $La(Mg_{1/2}Ti_{1/2})O_3$ in $BaTiO_3$ induces diffused phase transition, confirming the formation of polar nanoregions in the temperatures above T_C, thus causing coexistence of ferroelectric and relaxor states.
4. The relaxational behaviour of $BaBi_2Nb_2O_9$ ceramics is not typical for relaxors and the formalism developed for the dipolar glass is suitable for

the $BaBi_2Nb_2O_9$ ceramics, confirming the similar origin of dipolar glass and relaxor states.

Publications on the subject of doctoral thesis:

P1. P. Keburis, J. Banys, J.Grigas, A. Brilingas, T. Burtilius, A. N. Salak, V. M. Ferreira. Dielectric Properties of BT – LMT Mixed Ceramics. *Journal of the European Ceramic Society 27, 2007, p. 4367–4370.*

P2. P. Keburis, J. Banys, A. Brilingas, J. Prapuolenis, A. L. Kholkin and M.E.V. Costa. Dielectric Properties of Relaxor Ceramics BBN. *Ferroelectrics, Vol 353, 2007, p. 141-153.*

P3. P. Keburis, J. Banys, A. Brilingas, A. L. Kholkin and M.E.V. Costa. Dynamics of Nano Clasters in Ferroelectric Relaxor Ceramics BBN. *Nanosystems, Nanomaterials, Nanotechnologies, m. 5, № 2, 2007, p. 617–622.*

P4. P. Keburis, J. Banys, J.Grigas, Z. Bortkevic, A. L. Kholkin and M.E.V. Costa. Dielectric Properties of Relaxor Ceramics BBT. *Ferroelectrics, Vol 347, 2007, p.50-54.*

P5. P. Keburis, J. Banys, A. Brilingas, Z. Bortkevic, A. L. Kholkin and M.E.V. Costa. Dielectric Dispersion and Distribution of the Relaxation Times of The Relaxor Ceramics BBT. *Ferroelectrics, Vol 353, 2007, p. 87-90.*

P6. P. Keburis, D. A. Kiselev, J. Banys, M. E. V. Costa and A. L. Kholkin. PFM Studies of Domain Structure of Relaxor Ceramics $BaBi_2Nb_2O_9$. *J.G.Heinrich and C. Aneziris, Proc. 10th ECerS Conf., GöllerVerlag, Baden-Baden, 2007, p. 587-589.*

P7. V. V. Shvartsman, J. Dec, Z. K. Xu, J. Banys, P. Keburis and W. Kleemann. Crossover from ferroelectric to relaxor behaviour in BaTiSnO3 solid solutions. *Phase Transitions, Volume 81, Issue 11-12, 2008, p. 1013-1021.*

P8. J. Banys, R. Grigalaitis, A. Mikonis, J. Macutkevic and P. Keburis. Distribution of relaxation times of relaxors: comparison with dipolar glasses. *Phys. Status Solidi C, Volume 6, Issue 12, 2009, p. 2725-2730.*

Other publications:

P9. J. Grigas, A. Kania, J. Banys, A. Brilingas and P. Keburis. Relaxational dynamics of ferroelectric ALN ceramics at M_1-M_2 phase transition. *Lithuanian Journal of Physics, Vol. 43, No. 1, 2003, p. 59-64.*

P10. V. Samulionis, A. Salak, J. Banys, V. M. Ferreira and P. Keburis. Investigation of ultrasonic, dielectric and piezoelectric properties of the xLMT - (1-x)BT ceramics with x=0.025, 0.05, 0.075, 0.1. *Ultragarsas Vol 62, No 2, 2007, p. 7-10.*

P11. V. Samulionis, A. Salak, J. Banys, V.M. Ferreira and P. Keburis. Ultrasonic and piezoelectric properties of the BT–LMT ceramic system. *Journal of the European Ceramic Society*, *Volume 27, Issues 13-15*, *2007*, *p. 4003-4006*.

The results were presented in the following scientific conferences:

C1. P. Keburis, J. Banys, A. Brilingas, J. Prapuolenis, A. Kholkin, M. Costa. Dielectric properties of BBN ceramics // International meeting on clusters and nanostructured materials (CNM' 2006), Uzhgorod, Ukraine, October 9-12, 2006 : materials of the meeting. Uzhgorod, 2006, p. 161.

C2. J. Grigas, J. Banys, A. Brilingas, R. Grigalaitis, P. Keburis. Dielectric spectroscopy of clusters in nanostructured ceramics // International meeting on clusters and nanostructured materials (CNM' 2006), Uzhgorod, Ukraine, October 9-12, 2006 : materials of the meeting. Uzhgorod, 2006, p. 8-9.

C3. P. Keburis, J. Banys, A. Brilingas, Z. Bortkevič, A. Kholkin, M. Costa. Dielectric properties of 0,25 BBT - 0,75 SBT ceramics // Advanced materials as studied by spectroscopic and diffraction techniques : specialized colloque AMPERE and Alexander von Humboldt workshop, September 16-21, 2006, Vilnius, Lithuania : programme and abstracts. Vilnius, 2006, p. P41.

C4. P. Keburis, J. Banys, Z. Bortkevič, M. Costa, A. Kholkin, J. Grigas. Dielectric spectroscopy of BaBi2TaO9 (BBT) ceramics // RCBJSF-8: The 8th Russia/CIS/Baltic/Japan symposium on ferroelectricity, May 15-19, 2006, Tsukuba: abstract book. Tsukuba, 2006, p. 125.

C5. P. Keburis, J. Banys, A. Brilingas, A. Salak, V. Ferreira. Dielectric dispersion of LMT-BT ceramics // Functional materials and nanotechnologies (FM&NT-2006): 2nd Latvian conference, Riga, March 27-28, 2006. Riga, 2006, p. 28.

C6. P. Keburis, J. Banys, A. Brilingas, A. Kholkin. Dielectric properties of BBN ceramics // ECAPD'8 : 8th European conference on applications of polar dielectrics, Metz (France), September 5-8, 2006 : abstract book. Metz, 2006, p. 299.

C7. P. Keburis, J. Banys, A. Brilingas, Z. Bortkevič, A. Kholkin. Dielectric properties of BBT ceramics // ECAPD'8 : 8th European conference on

applications of polar dielectrics, Metz (France), September 5-8, 2006 : abstract book. Metz, 2006, p. 214.

C8. P. Keburis, J. Banys, A. Brilingas, A. Salak, V. Ferreira. Dielectric properties of BT-LMT mixed ceramics // Verhandlungen der Deutschen Physikalischen Gesellschaft 2006, no 1, p. 134.

C9. P. Keburis, J. Banys, A. Brilingas, J. Grigas, A. Salak, V. Ferreira. Dielectric properties of BT-LMT mixed ceramics // Electroceramics: Toledo, 6 (18-22 June,2006): book of abstracts. Toledo, 2006, p. 247.

C10. P. Keburis, J. Banys, Z. Bortkevič, J. Grigas, A. Kholkin. Dielectric properties of lead free ceramics BBT // Functional materials and nanotechnologies (FM&NT-2006): 2nd Latvian conference, Riga, March 27-28, 2006. Riga, 2006, p. 29.

C11. J. Banys, V. Samulionis, A. Salak, V. Ferreira, P. Keburis. Electrostriction induced piezoelectricity and memory effects in BT-LMT ceramics // Electroceramics: Toledo, 6 (18-22 June,2006): book of abstracts. Toledo, 2006, p. 263.

C12. V. Samulionis, A. Salak, J. Banys, V. Ferreira, P. Keburis. Ultrasonic and piezoelectric properties of the BT-LMT ceramic system // Electroceramics: Toledo, 6 (18-22 June,2006): book of abstracts. Toledo, 2006, p. 270.

C13. P. Keburis, J. Banys, A. Brilingas, A. Kholkin, M. Costa. Dielectric spectroscopy of BaBi2Ta2O9 (BBT) ceramics // 37-oji Lietuvos nacionalinė fizikos konferencija : programa ir pranešimų tezės, Vilnius, 2007 m. birželio 11-13. Vilnius : [Vilniaus universitetas], 2007, p. 78.

C14. J. Banys, V. Samulionis, P. Keburis, A. Salak, V. Ferreira. Electrostriction induced piezoelectricity and memory effects in BT-LMT ceramics // 37-oji Lietuvos nacionalinė fizikos konferencija : programa ir pranešimų tezės, Vilnius, 2007 m. birželio 11-13. Vilnius : [Vilniaus universitetas], 2007, p. 76.

C15. P. Keburis, J. Banys, A. Brilingas, J. Prapuolenis, A. Kholkin, M. Costa. Investigation of dielectric properties of BBN Ceramics // 37-oji Lietuvos

nacionalinė fizikos konferencija : programa ir pranešimų tezės, Vilnius, 2007 m. birželio 11-13. Vilnius : [Vilniaus universitetas], 2007, p. 77.

C16. J. Banys, V. Samulionis, A. Salak, V. Ferreira, P. Keburis. Investigation of lead-free BT-LMT ceramics for ultrasonic transducers // 37-oji Lietuvos nacionalinė fizikos konferencija : programa ir pranešimų tezės, Vilnius, 2007 m. birželio 11-13. Vilnius : [Vilniaus universitetas], 2007, p. 74.

C17. P. Keburis, J. Banys, A. Brilingas, A. Kholkin, M. Costa. Dielectric properties of 0,25 BBT- 0,75 SBT ceramics // Functional materials and nanotechnologies (FM&NT-2007): international Baltic Sea region conference, Riga, April 24, 2007: book of abstracts. Riga, 2007, p. 96.

C18. P. Keburis, J. Banys, A. Brilingas, V. Shvartsman, W. Kleemann, S. Lu. Dielectric properties of BaTi0.9Sn0.1O3 ceramics // EMF-2007 : 11th European meeting on ferroelectricity, Slovenia, 3-7 September 2007 : programme and book of abstracts. Bled, 2007, p. 48.

C19. J. Banys, R. Grigalaitis, P. Keburis, A. Džiaugys, A. Mikonis. Dielectric relaxation in ferroelectrics, relaxors and dipolar glasses // Seminar properties of ferroelectric and superionic systems, Ukraine, 12-13 November, 2007. Uzhgorod, 2007, p. 16.

C20. P. Keburis, J. Banys, A. Kholkin, M. Costa. Oxygen vacancies conductivity in relaxor ceramics BaBi2Ta2O9 // 8th international symposium on systems with fast ionic transport: book of abstracts, Vilnius, 23-27 May, 2007. Vilnius, 2007, p. [].

C21. Keburis Povilas, Banys Jūras, Brilingas Algirdas, Prapuolenis Jonas, Samulionis Vytautas, Kholkin Andrei L. , Costa Maria Elisabete. Dielectric spectroscopy of 0.75 BBN - 0.25 SBN ceramics // ICE 2007 : international conference on electroceramics : program and abstracts,31 July - 3 August, 2007, Tanzania. Arusha, 2007, p. 73.

C22. Banys Jūras, Keburis Povilas, Salak Andrei N. , Ferreira Victor M. , Samulionis Vytautas. Investigation of lead BT-LMT ceramics for ultrasonic transducers // ICU 2007 : International congress on ultrasonics :

program and book of abstracts, Vienna, April 9-12, 2007. Vienna, 2007, p. 116.

C23. Keburis Povilas, Kiselev D. A. , Banys Jūras, Costa Maria Elisabete, Kholkin Andrei L. PFM studies of domain structure of relaxor ceramics BaBi2Nb2O9 // 10th international conference and exibition of the European ceramic society : programme [and abstracts book], Berlin, June 17-21, 2007. Berlin, 2007, p.

C24. Keburis Povilas, Banys Jūras, Brilingas Algirdas, Lekstutis Andrius, Salak Andrei N. , Ferreira Victor M. Dielectric spectra of lead-free ceramics (1-x)BaTiO3-x La(MG1/2Ti1/2)O3 (BT-LMT) with x=0.05 // Smart materials and structures: 2nd international workshop, Kiel, 2007, 29-31 August. Kiel, 2007, p. 127.

C25. Salak Andrei N. , Vyshatko Nikolai P. , Kholkin Andrei L. , Olekhnovich Nikolai M. , Radyush Yury V. , Pushkarou Anatoly V. , Keburis Povilas, Banys Jūras, Samulionis Vytautas, Ferreira Victor M. Dielectric and electromechanical properties of the lead-free relaxor ferroelectric ceramics in the (Na1/2Bi1/2)TiO3 system // RCBJSF-9: the 9th Russian-CIS-Baltic-Japan Symposium on Ferroelectricity, Vilnius, Lithuania, June 15-19, 2008 : abstract book. Vilnius, 2008, p. 143.

C26. Keburis Povilas, Banys Jūras, Brilingas Algirdas, Shvartsman V. V. , Kleemann Wolfgan, Lu S. G. Dielectric investigations of BaTi1-xSnxO3 ceramics // RCBJSF-9: the 9th Russian-CIS-Baltic-Japan Symposium on Ferroelectricity, Vilnius, Lithuania, June 15-19, 2008 : abstract book. Vilnius, 2008, p. 92.

C27. Keburis Povilas, Banys Jūras, Brilingas Algirdas, Salak Andrei N. , Ferreira Victor M. Broadband dielectric spectra of 0.95 BaTiO3-0.05 La(Mg1/2Ti1/2)O3 ceramics // COST 539 action - ELENA : 4th workshop "Fabrication, properties and applications of electroceramic nanostructures" : programme and book of abstracts, Genoa, Italy, June 26-28, 2008. Genoa, 2008, p. 55.

C28. Keburis Povilas, Banys Jūras, Brilingas Algirdas, Shvartsman V. V. , Kleemann Wolfgan, Lu S. G. Dielectric properties of BaTi0.75Sn0.25O3 ceramics // ECAPD'9 : 9th European conference on applications of polar dielectrics, Roma, Italy, August 25-29, 2008 : abstract book. Roma, 2008, p. 139.

C29. Keburis Povilas, Banys Jūras, Kholkin Andrei L. , Costa Maria Elisabete, Grigas Jonas. Dielectric studies of 0.5 SBT-0.5 BBT ceramics // Electroceramics XI: Manchester, 31st August-4th September 2008 : book of abstracts. Manchester, 2008, p. N-031-P.

C30. Banys Jūras, Grigalaitis Robertas, Mikonis Andrejus, Keburis Povilas. Distribution of relaxation times of relaxors comparison with dipolar glasses // 15th semiconducting and insulating materials conference, June 15-19, Vilnius, Lithuania : programme and abstracts. Vilnius, 2009, p. 46.

C31. Keburis Povilas, Banys Jūras, Brilingas Algirdas, Kholkin Andrei L. , Costa Maria Elisabete. Local order parameter behaviour of BBN relaxor ceramics evidenced from dielectric spectroscopy // 15th semiconducting and insulating materials conference, June 15-19, Vilnius, Lithuania : programme and abstracts. Vilnius, 2009, p. 114.

C32. Keburis Povilas, Banys Jūras, Brilingas Algirdas, Kholkin Andrei L. , Costa Maria Elisabete. Dipolar behaviour of BaBi2Nb2O9 relaxor evidenced from dielectric spectroscopy // COST 539 action - ELENA : programme and book of extended abstracts of 2nd training school and 6th workshop "Advance functional characterization of nanostructured materials, Madrid, Spain, February 23-25, 2009. Madrid, 2009, p. 60-61.

C33. Banys Jūras, Grigalaitis Robertas, Mikonis Andrejus, Keburis Povilas. Dielectric spectroscopy of dipolar glasses and relaxors - comparison of distribution of relaxation times // ICE 2009 : international conference on electroceramics : abstracts, 13-17th December, 2009, Delhi, India. Delhi, 2009, p. 52.

C34. Banys Jūras, Grigalaitis Robertas, Mikonis Andrejus, Keburis Povilas, Macutkevič Jan. Dielectric spectroscopy of relaxors and dipolar glasses -

are they the same? // IMF -ISAF 2009 : 12th international meeting on feroelectricity and 18th IEEE international symposium on the applications of ferrpelectric : program abstracts book, August 23-27, Xi'an, China. Xi'an, 2009, p. 16.

C35. Keburis Povilas, Banys Jūras, Brilingas Algirdas, Salak Andrei N. , Ferreira Victor M. Dielectric spectra of barium titanate doped with lanthanum magnesium titanate // Functional materials and nanotechnologies (FM&NT-2010) : international conference, Riga, March 16-19 : book of abstracts. Riga : Latgales druka, 2010, p. 99.

1. LITERATURE OVERVIEW

1.1. Relaxor ferroelectrics

Relaxor ferroelectrics (RLs) include a large group of solid solutions, mostly oxides, with a perovskite or tungsten bronze structure. In contrast to ordinary ferroelectrics (FE) whose physical properties are quite adequately described by the Landau-Ginzburg-Devonshire theory [24], RLs possess the following main features: (i) a significant frequency-dependence of the dielectric permittivity, (ii) absence of both spontaneous polarization and structural macroscopic symmetry breaking, (iii) ferroelectric-like response arising after field cooling to low temperature [25]. Figure 1.1 shows the most prominent differences between normal (FE) and relaxor (RL) ferroelectrics:

a) The FE polarization (P) versus electric field (E) hysteresis loop is nearly of square shape and shows large remanent polarization, P_R, due to the switching of macroscopic long-range ordered domains. A RL shows a so-called slim loop, which indicates that the long-range ordering needs large fields, while in zero field the polarization decays into submicroscopic nanoregions, which re-acquire their natural random orientations, resulting in small P_R values.

b) Saturation and remanent polarization of a FE decrease with increasing temperature and vanish at the phase transition temperature T_C. No polar domains exist above T_C. By contrast, the field-induced polarization of a RL decreases smoothly through the dynamic transition temperature T_m and retains finite values up to rather high temperatures due to the fact that the nanopolar domains persist to well above T_m.

c) 1) The static dielectric susceptibility χ' or dielectric permittivity $\varepsilon' = 1 + \chi'$ of a FE exhibits a sharp and narrow peak at T_C (FWUM ≈ 10 – 20 K) with frequency independence in the audio range. By contrast RLs exhibit a very broad peak and a strong frequency dispersion in both position (T_m) and height (ε'_{max}) of the anomaly.

2) The T dependence of ε' of a FE obeys a Curie-Weiss law, $\varepsilon' = C/(T - T_0)$, above T_C as shown by a linear relationship of $1 / \varepsilon'$ versus T. By contrast $\varepsilon'(T)$ of a RL exhibits strong deviation from Curie-Weiss behaviour well above T_m.

d) The existence of a macroscopic symmetry change for a FE at T_C, give rise to usual phase transition features with changes of the refractive properties (occurrence or drastic change of birefringence), while in the absence of macroscopic symmetry breaking no such phenomena are observed in a RL at T_m.

Very high response coefficients and the enhanced width of the high response regime around the "ordering" temperature T_m, ("Curie range") make RLs popular systems for applications as piezoelectric/electrostrictive *actuators* and *sensors* (e.g. scanning probe microscopy, ink jet printer, adaptive optics, micromotors, vibration sensors/attenuators, Hubble telescope correction, ...) and as *electro-* or *elasto-optic and photorefractive elements* (segmented displays, modulators, image storage, holographic data storage,...). When reflecting on the occurrence of RL behaviour in perovskites, there appear to be three essential ingredients:

- existence of *lattice disorder,*
- existence of *polar nanoregions* at temperatures much higher than T_m,
- residence of these domains within the *highly polarizable host lattice* governed by a soft optic mode.

The first ingredient can be taken for granted, since RL behaviour in these materials does not occur in the absence of disorder. The third ingredient is also an experimental fact in that RL behaviour occurs in ABO_3 oxides with very large dielectric permittivities.

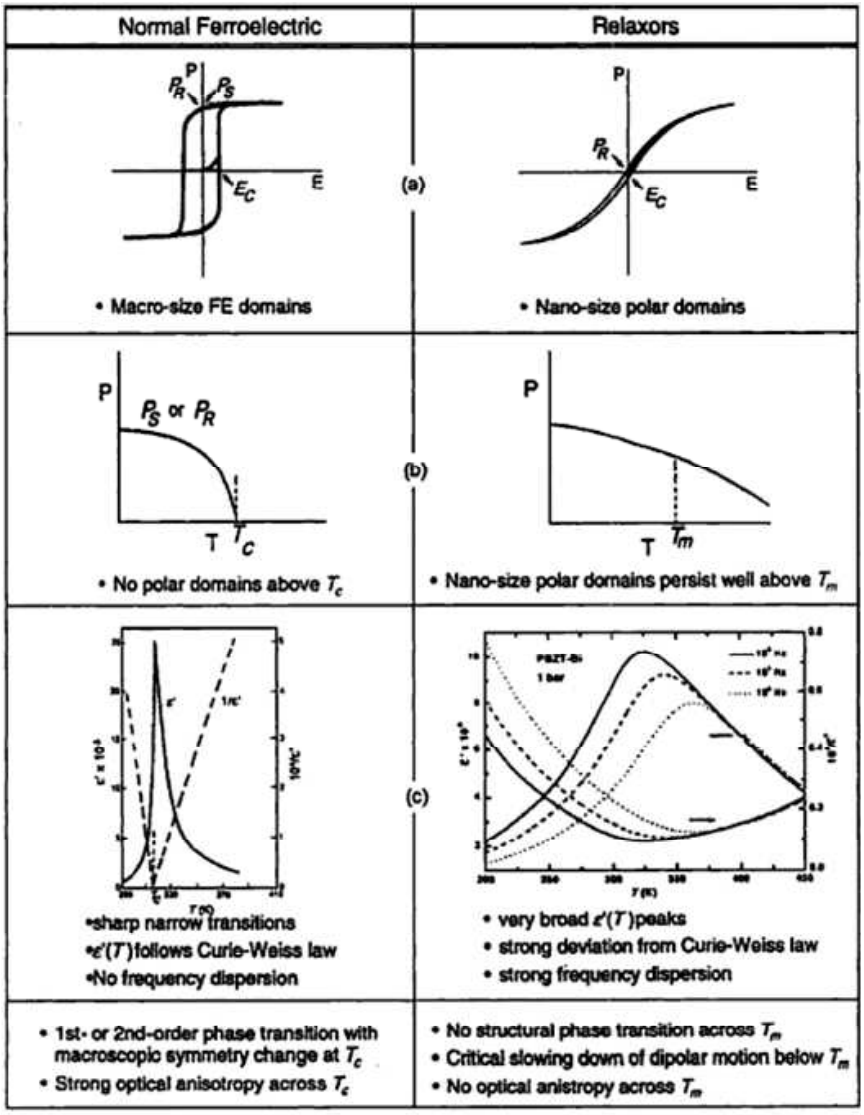

Fig. 1.1. Different properties of normal ferroelectrics and relaxor ferroelectrics or relaxors [25].

The second ingredient manifestes itself in many experimental observations in all perovskite RLs, as will be discussed later.

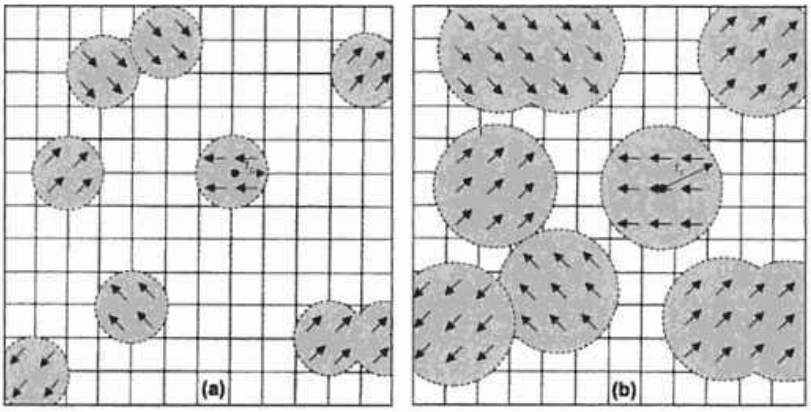

Fig. 1.2. Randomly distributed dipolar domains in soft-mode host lattice. At high temperature (but below T_d) the domains and the correlation radius, r_c, are small (a), both grow and coalesce at low temperatures (b).

The following physical picture has emerged for RLs and has become generally accepted. Chemical substitution and lattice defects introduce dipolar entities in mixed ABO_3 perovskites. At very high temperatures, thermal fluctuations are so large that there are no well-defined dipole moments. However, on cooling, the presence of these dipolar entities manifests itself as smals polar nanoregions (Fig 1.2) below the so-called Burns temperature, T_d [26]. These domains grow as the correlation length, r_c, increases with decreasing T, and ultimately, one of two things happens. If the domains become large enough (macrodomains) so as to percolate (or permeate) the whole sample, then the sample will undergo a static, cooperative FE phase transition at T_C. On the other hand, if the nanoregions grow with decreasing T but do not become large enough or percolate the sample, then they will ultimately exhibit a dynamic slowing down of their fluctuations at $T < T_m$ leading to an isotropic RL state with random orientation of the polar domains.

A matter of dispute is still the relevance and the very origin of the Burns temperature. Very probably this is not a usual phase transitions temperature. It might rather be considered as a so-called Griffiths temperature, which signifies

the onset of weak singularities in a diluted ferroic system below the transition temperature of the undiluted system [27,28]. However, the sharp onset of weak singularities is not at all confirmed in RL systems. We rather believe that the temperature regime in which the domains grow in size is a continuous one, which is determined by the correlating forces due to the underlying quenched random field (*RF*) distribution [29] .

Another characteristic relaxor property is the extremely slow relaxation below T_m, which signals the onset of relaxor freezing [13]. The characteristic relaxation time diverges at the freezing temperature T_0 according to the well-known Vogel–Fulcher (VF) relation [30,31]

$$\tau = \tau_0 \exp [U/k (T - T_0)] \qquad (1.1)$$

where τ_0 represents the inverse attempt frequency, U the activation energy, and T_0 the VF or freezing temperature. For obvious reasons, Eq. 1.1 only makes sense for $T > T_0$.

The above empirical VF law (1.1) has been experimentally observed in a variety of other systems such as supercooled organic liquids, spin glasses, polymers, etc. Although many theoretical ideas about the origin of the VF law have been proposed in the past, a derivation of Eq. 1.1 at the mesoscopic level is still lacking.

The above describes the situation in the absence of a biasing electric field. Cooling in the presence of a biasing field, however, aligns the domains and increases their correlation length, effectively canceling the influence of the *RFs*. For sufficiently large E_{bias} the domains become large leading to the onset of long-range FE order. This is a field-induced nano-to-macrodomain transition. This transition occurs spontaneously in some cases in the absence of bias (e.g. for $Pb_{1-y}La_yZr_{1-x}Ti_xO_3$, PLZT). Evidence for the nano-to-macrodomain transition in RLs can be inferred, as we shall see, from the dielectric response and can often be seen in TEM images and from scattering data [32]. Its occurrence is determined by a delicate balance among E_{bias},

thermal fluctuations and the strength of dipolar correlations. Much insight about the physics of RLs has been gained from measurements in the presence *dc* bias. Such measurements lead to distinct behaviour as shown for $\varepsilon'(T)$ in Figure 1.3.

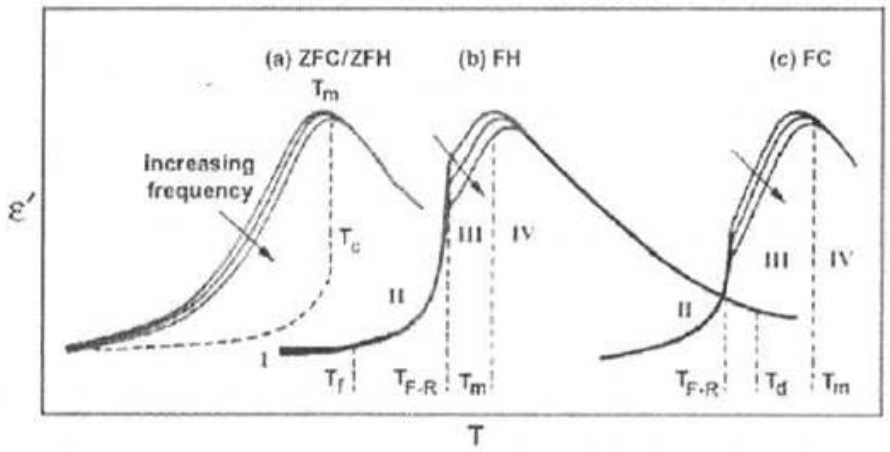

Fig. 1.3. Dielectric response of RLs both without and with electric field bias as discussed in the text. Response (b) defines all the various characteristic "transition" temperatures of RL [33].

Figure 1.3(a) is the signature of a RL in the absence of bias. The same relaxational response is observed under both zero-field cooling (ZFC) and zero-field heating (ZFH) conditions. The dashed curve depicts the field-induced, frequency-independent FE response for sufficiently large E_{bias} which stabilizes the FE phase at low temperatures. Figure 1.3(b) and (c) show the responses for intermediate biases. For field heating (FH) conditions after ZFC, the response has four regions (Figure 1.3(b)). Region I is a dispersive region consisting of frozen-in, randomly oriented nanoregions. Below T_f (a freezing temperature) there is not enough thermal energy to unfreeze and align the domains with the field. However, at $T > T_f$ (region II) the nanoregions align and grow, forming macrodomains. This is a dispersion free FE region. On further heating, a temperature, $T_{F\text{-}R}$, is reached above which thermal

fluctuations become sufficiently large so as to break the ordering tendency of the intermediate strength biasing field. As a result, the macrodomains break into randomly oriented, slowed down nanoregions, i.e., a dispersive RL state (region III). Finally, above T_m the sample enters the PE state (region IV) where the nanoregions undergo rapid thermal fluctuations.

Also in Figure 1.3(b) is shown the fourth characteristic temperature, the Burns temperature, T_d ($> T_m$), where nanoregions first nucleate. Figure 1.3(c) shows the response of the sample under field cooling (FC) conditions for intermediate strength fields. Regions IV and III are similar to those in Figure 1.3(b). However, at $T \leq T_{F\text{-}R}$ the behaviour is different. Here the field aligns and grows the nanoregions into macrodomains (a FE state). Once aligned, the macrodomains remain aligned and stable down to the lowest temperature in the presence of the field. Thus region I is absent in this case.

1.2. Dipolar glasses

Orientational glasses (dipolar, quadrupolar or octupolar) are crystalline materials that transform from a high-temperature crystalline phase into a low-temperature glassy state. Analogous to the spin glasses (for a review see Ref. [34]), randomly substituted impurity ions (or molecules) that carry a dipolar moment are located on a topologically ordered lattice. These moments have orientational degrees of freedom and they interact with one another. The dominant exchange interaction can be of electrostatic dipolar, quadrupolar or octupolar, or of elastic quadrupolar nature. In the latter case, the interaction is mediated via lattice strains. Due to site disorder and anisotropic interactions, the orientational disorder is cooperatively frozen-in. The use of the term "glass-state" suggests some similarity with canonical glasses such as vitreous silica. Indeed, the orientational glasses exhibit relaxation dynamics similar to those observed in canonical glasses. In addition, the low-temperature thermodynamic, elastic and dielectric properties are characteristic of

amorphous systems. Well-known examples are mixtures of ferroelectric and antiferroelectric compounds such as rubidium ammonium dihydrogen phosphate (RADP) [35] (Fig. 1.4) and mixtures of the elastically ordered KCN and NaCN [34].

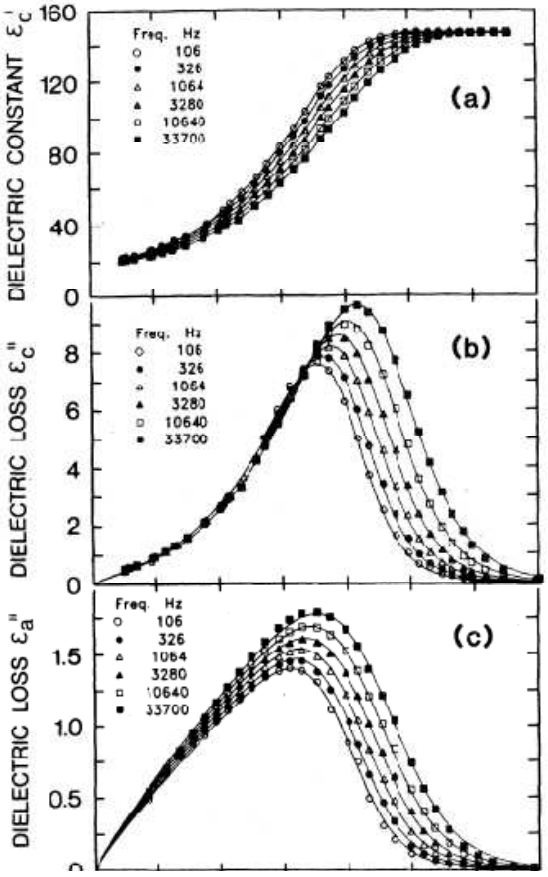

Fig. 1.4. (a) The real part of dielectric permitivity ε'_c. (b) The imaginary parts of dielectric permittivity ε_c'' (longitudal) and ε_a'' (transverse) of RAPD.

In RADP, a frustrated ground state is believed to occur via the competing electrical interactions. In NaCN:KCN, it seems plausible that the random fields suppress a long-range elastic order [35]: random strains are introduced by the volume difference of the impurity atoms that cause quenched elastic relaxations of the neighbouring ions.

1.3.Polar nanoregions

While many researchers believe that the above mentioned three ingredients for *RL* behaviour to appear are more or less independent, the arguements have been made since long [29] that the primary cause of *RL* behaviour is the lattice disorder, which is at the origin of the occurrence of polar nanoregions and their fluctuations within the highly polarizable lattice. In order to describe disordered systems and to explore their basic thermodynamic behaviour simple spin models are frequently used.

The model Hamiltonian $H = -\sum_{ij} J_{ij} S_i S_j - \sum_i h_i S_i$ (1.2)

accounts for random interactions (or random bonds, *RB*s), J_{ij}, between nearest neighbour spins S_i and S_j, and for quenched random fields *(RFs),* h_i acting on the spins S_i. While the *RBs* are at the origin of spin glass behaviour [34], *RFs* may give rise to disordered domain states provided that the order parameter has continuous symmetry [36]. This is easily shown with the help of energy arguments considering both the bulk energy decrease by fluctuations of the *RFs* and the energy increase due to the formation of domain walls. A remarkable exception, which does not necessarily lead to a disordered ground state, is the random-field Ising model (*RFIM)* system. Owing to its discontinuous spin symmetry, atomically thin domain walls are expected, which are energetically unfavorable. For this reason the three-dimensional (*3d*) *RFIM* is expected to exhibit long-range order below the critical temperature T_C. However, as a tribute to the *RFs* new criticality due to a $T = 0$ fixed point [37] and strongly decelerated critical dynamics are encountered [38].

Evidence for the existence of polar nanoregions well above T_m has come from high resolution TEM which also showed the growth of these domains with decreasing T [33]. The evidence is also prominently reflected in certain properties of these systems.

The manifestation of the presence of polar nanoregions in strong RLs in terms of the electrooptic effect was first demonstrated by Burns and Dacol [39] in

measurements of the T dependence of the refractive index, n. For a normal ABO_3 FE crystal, starting in the high-temperature PE phase, n decreases linearly with decreasing T down to T_b, at which point n deviates from linearity. The deviation is proportional to the square of the polarization and increases as the polarization evolves with decreasing T. If the FE transition is of the first order, then there is a discontinuity in n at T_C followed by the expected deviation. This qualitative picture is representative of the behaviour of many perovskite FEs. However, in the case of RLs, Burns and Dacol observed deviation from linear $n(T)$ well above T_m.

Deviation from the Curie-Weiss behaviour is commonly observed in the temperature dependence of the magnetic susceptibility, χ, of spin glasses [34] above the freezing temperature of spin fluctuations, T_f (which corresponds to T_d for RLs in some sense). Also in an ideal superparamagnet, i.e., in non-interacting paramagnetic particles or clusters, $\chi(T)$ exhibits Curie-Weiss behaviour. This behaviour is achieved in spin glasses for high temperatures compared to T_f. At lower temperatures, deviation from the Curie-Weiss law is attributed to strong local magnetic correlations [34] and the onset of local (spin-glass) order below T_f. Sherrington and Kirkpatrick [40] developed a model, which relates $\chi(T)$ below T_f to the local order parameter q:

$$\chi = \frac{C\,(1-q(T))}{T-\theta(1-q(T))} \qquad (1.3)$$

where q is a function of temperature. Clearly q and its temperature dependence can be evaluated from $\chi(T)$ data and the values of C and θ determined from the high-temperature $\chi(T)$ response above T_f which follows the Curie-Weiss law. In this high-temperature regime q —> 0 and Eq. (1.3) simply reduces to the Curie-Weiss form. Eq. (1.3) can be thought of as a modified Curie-Weiss law where both C and θ are functions of temperature. If we presume that the deviation from the Curie-Weiss behaviour in PMN and other RLs is due to correlations among local nanoregions, then we may evoke Eq. (1.3) to treat the high-temperature dielectric response of RLs. Indeed this equation has been

shown to provide a satisfactory description of the $\chi(T)$ response of RLs [41,42]. As expected, q —> 0 above, e.g., around 625 K for PMN, and it increases with decreasing temperature below T_d because of increased dipolar correlations [41]. In such a case the local order parameter due to correlations between neighbouring polar domains of polarization P_i and P_j is $q=< P_iP_j >^{1/2}$.

1.4. Perovskites

A very important group of ferroelectrics is known as the perovskites from the mineral perovskite $CaTiO_3$ (which itself is actually a distorted perovskite structure) [24]. The perfect perovskite structure is extremely simple one with general formula ABO_3, where A is monovalent or divalent metal and B is tetra or pentavalent one (Fig 1.5). It is cubic, with the A atoms at the cube corners, B atoms at the body centers and the oxygens at the face centres.

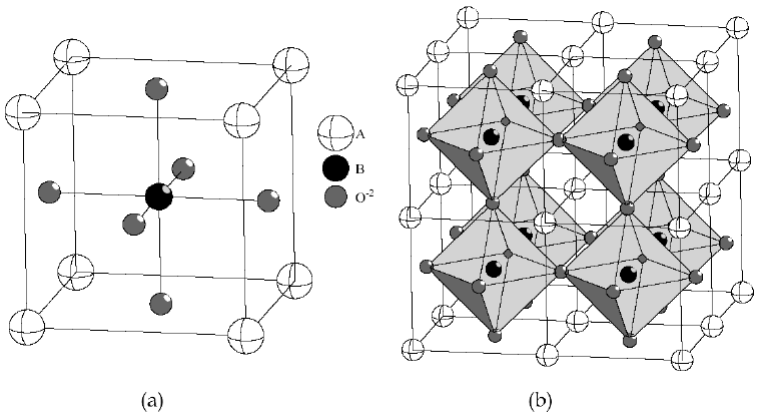

Fig. 1.5. The cubic ABO_3 structure (a) unite cell and (b) octahedra framework [24].

Many piezoelectric (including ferroelectric) ceramics such as Barium Titanate ($BaTiO_3$), Lead Titanate ($PbTiO_3$), Lead Zirconate Titanate (PZT), Lead Lanthanum Zirconate Titanate (PLZT), Lead Magnesium Niobate (PMN), Potassium Niobate ($KNbO_3$), Potassium Sodium Niobate ($K_xNa_{1-x}NbO_3$),

Potassium Tantalate Niobate ($K(Ta_xNb_{1-x})O_3$) and many others have a perovskite type structure.

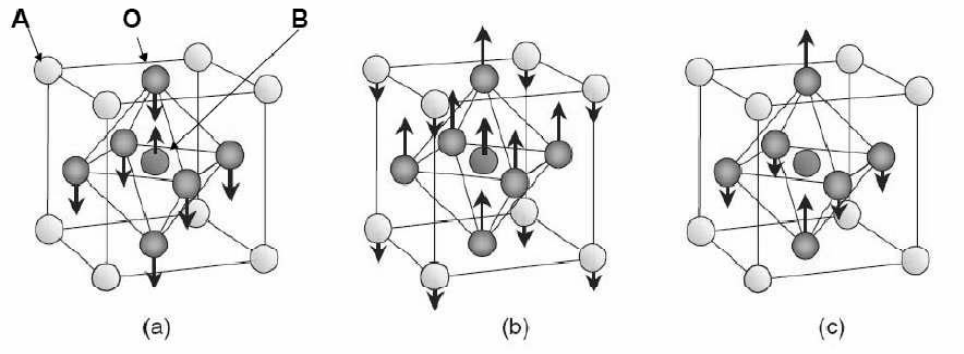

Fig. 1.6. IR active normal modes in simple cubic perovskites ABO_3: (a) Slater mode, (b) Last mode and (c) Axe mode.

First discovered perovskite ferroelectric material - Barium titanate ($BaTiO_3$) has a paraelectric cubic phase above its Curie point of about 130° C. In the temperature range of 130° C to 0° C the ferroelectric tetragonal phase with a c/a ratio of ~ 1.01 is stable. The spontaneous polarization is along one of the [001] directions in the original cubic structure. Between 0° C and -90° C, the ferroelectric orthorhombic phase is stable with the polarization along one of the [110] directions in the original cubic structure. On decreasing the temperature below -90° C the phase transition from the orthorhombic to ferroelectric rhombohedral phase leads to polarization along one of the [111] cubic directions.

The spontaneous polarization on cooling $BaTiO_3$ below the Curie point T_c is due to changes in the crystal structure. As shown in Fig. 1.7 the paraelectric cubic phase is stable above 130° C with the center of positive charges (Ba^{2+} and Ti^{4+} ions) coinciding with the center of negative charge (O^{2-}).

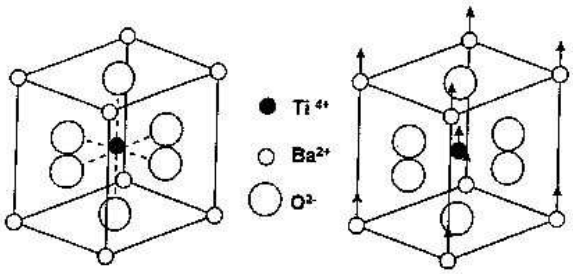

Fig. 1.7. The crystal structure of $BaTiO_3$ (a) above the Curie point the cell is cubic; (b) below the Curie point the structure is tetragonal with Ba^{2+} and Ti^{4+} ions displaced relative to O^{2-} ions.

On cooling below the Curie point T_c, a tetragonal structure develops where the center of Ba^{2+} and Ti^{4+} ions are displaced relative to the O^{2-} ions, leading to the formation of electric dipoles. Spontaneous polarization developed is the net dipole moment produced per unit volume for the dipoles pointing in a given direction.

The ferroelectric phase transition in $BaTiO_3$ is generally considered to be the classical example of a displacive soft-mode–type phase transition (Fig. 1.8 a) describable by anharmonic lattice dynamics [43,44].

The off-center displacements of Ti ions in the high temperature cubic phase of $BaTiO_3$ have recently been demonstrated by NMR experiments [45], which reveal that the order-disorder dynamics of Ti ions coexists with the observable displacive features of the TO soft mode (Fig. 1.8 b).

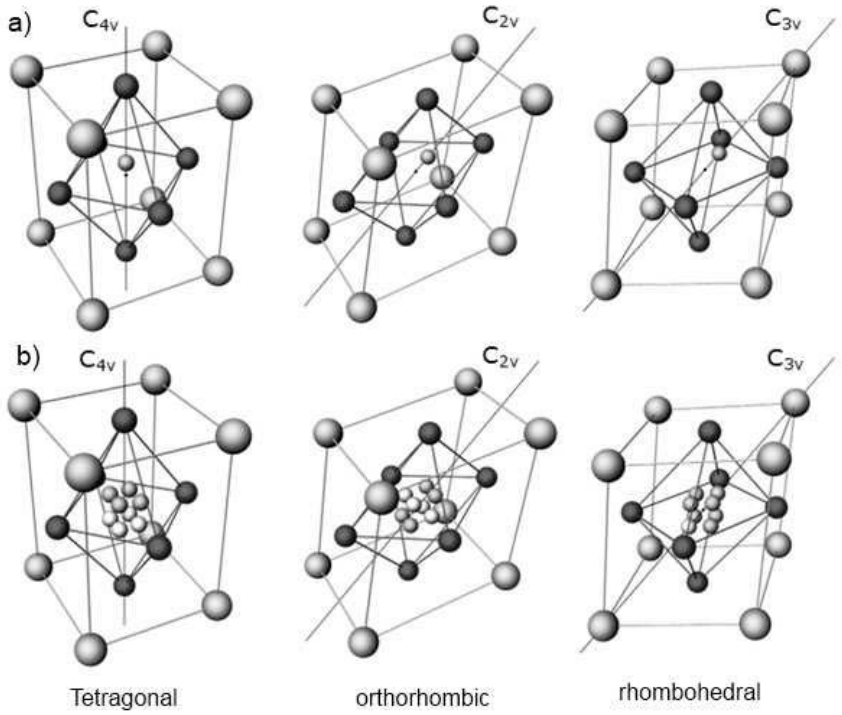

Fig. 1.8. $BaTiO_3$ undergoing phase transitions from tetragonal to orthorombic and rhombohedral in terms of a) displacive scenario – freezing of soft TO lattice mode and b) order-disorder scenario.

Various A and B site substitutions in different concentrations have been tried to see their effect on the dielectric and ferroelectric properties of $BaTiO_3$. Sr^{2+} substitutions to the A site have been found to reduce the Curie point linearly towards room temperature. The substitution of Pb^{2+} for Ba^{2+} raises the Curie point. The simultaneous substitution into both A and B sites with different ions can be used to tailor the properties of $BaTiO_3$. The effect of various isovalent substitutions on the transition temperatures of $BaTiO_3$ ceramic are shown in Fig. 1.9 [46].

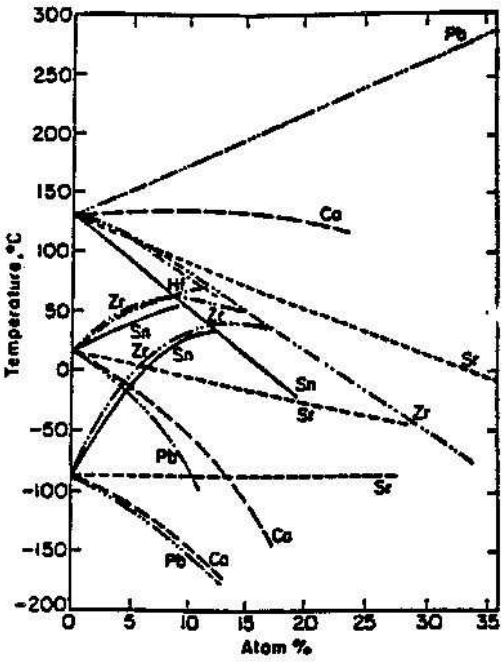

Fig. 1.9. The effect of isovalent substitutions on the transition temperatures of BT ceramics [46].

The dielectric properties of $BaTiO_3$ are found to be dependent on the grain size [47]. Figure 1.10 shows the variation of dielectric permittivity with temperature for $BaTiO_3$ ceramics with a fine (~ 1 μm) and coarse (~ 50 μm) grain size. Large grained $BaTiO_3$ (≥ 1 μm) shows an extremely high dielectric permittivity at the Curie point. This is because of the formation of multiple domains in a single grain, the motion of whose walls increases the dielectric permittivity at the Curie point. For a $BaTiO_3$ ceramics with fine grains (~ 1 μm), a single domain forms inside each grain. The movement of domain walls are restricted by the grain boundaries, thus leading to a low dielectric permittivity at the Curie point as compared to coarse grained $BaTiO_3$ [48]. The room temperature dielectric permittivity (ε_r) of coarse grained (≥ 10 μm) BT ceramics is found to be in the range of 1500-2000. On the other hand, fine grained (~1 μm) BT ceramics exhibit a room temperature dielectric permittivity between 3500-6000. The grain size effect on the dielectric

permittivity at room temperature has been explained by the work of Buessem et. al. [49] and Arlt et. al. [50]. Buessem and coworkers proposed that the internal stresses in fine grained $BaTiO_3$ must be much greater than the coarse grained ceramic, thus leading to a higher permittivity at room temperature.

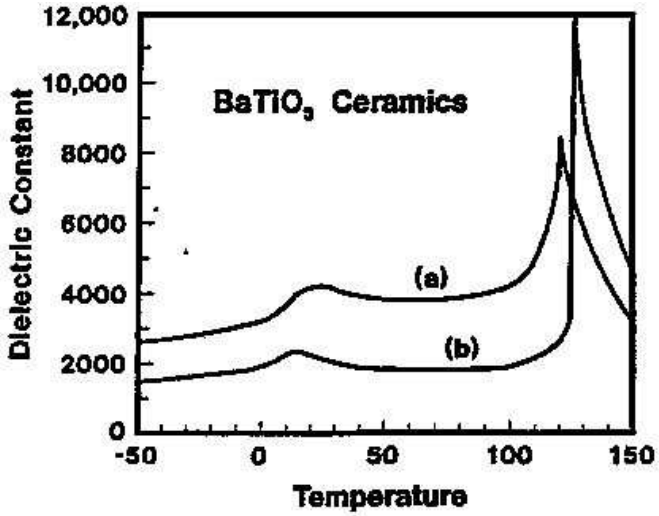

Fig. 1.10. The variation of the relative permittivity (ε_r) with temperature for BaTiO3 ceramics with (a) 1 μm grain size and (b) 50 μm grain size [29] (Temperature is ºC).

As already noted, in ferroelectrics relaxor behaviour results from either frustration or compositionally induced disorder [34]. This disorder and related random fields are believed to be responsible for the relaxor properties of the mixed ABO_3 perovskite oxides. In addition to a broad, frequency-dependent peak in $\varepsilon'(T)$ relaxors are characterized by the absence of macroscopic phase (symmetry) change at the transition. The parent compounds of ABO_3 perovskite relaxors (e.g. $BaTiO_3$, $PbTiO_3$, $PbZrO_3$, $KTaO_3$) are prototypical soft-mode systems whose dielectric properties and phase transitions are well understood in terms of soft phonon mode theory. A variety of types of disorder in this lattice can produce dipolar defects and induce relaxor behaviour. Properties of such mixed-compound ferroelectric ceramic materials will be discussed in the following chapters.

1.5.Dopped $BaTiO_3$ ferroelectric relaxor ceramics

In ferroelectric $BaTiO_3$ based materials the relaxor behaviour can be achieved not only in heterovalently substituted solid solutions [51-53], but also in isovalently substituted solid solutions, for example, in $BaTi_{1-x}Sn_xO_3$ [54-56]. The dielectric permittivity of the $(1-x)BaTiO_3 - xLa(Mg_{1/2}Ti_{1/2})O_3$ ceramics with different x – the example of heterovalent substitution is presented in Fig. 1.11. Even at low substitution rate (5%) only one clearly expressed phase transition is observed and authors of [53] suggest this to be the point of the crossover from ferroelectric to relaxor state (Fig. 1.12). In example of $BaTi_{1-x}Sn_xO_3$ ceramics [57], the compositions from the intermediate concentration range of 8%–20% show a behaviour being different from both the normal ferroelectrics and canonical relaxors. The dielectric permittivity exhibits a strongly diffused maximum (Fig. 1.13), but with a frequency independent position. Such behaviour is occasionally denoted as diffused phase transition (DPT) in order to distinguish it from the relaxor one. The interpretations of the nature of DPTs are controversial. Mueller *et al.* [58] attributed the DPT to a ferroelectric pase transition based on the observation of domains in compositions with Sn content less than 13% [59]. On the other hand, Wei *et al.* [54] proposed that DPTs already correspond to the relaxor state, and the distinction between frequency independent DPT and frequency dependent relaxorlike behaviours is due to the different sizes of the PNRs with the consequence of different relaxation frequencies. When these relaxation frequencies are close to the experimental ones, relaxor behaviour is observed; when they are far from the experimental ones, only DPT behaviour is expected [57].

In order to explain the appearance of relaxor properties in $BaTiO_3$-based compositions, several other models were proposed which were all based on the internal heterogeneity of these materials.

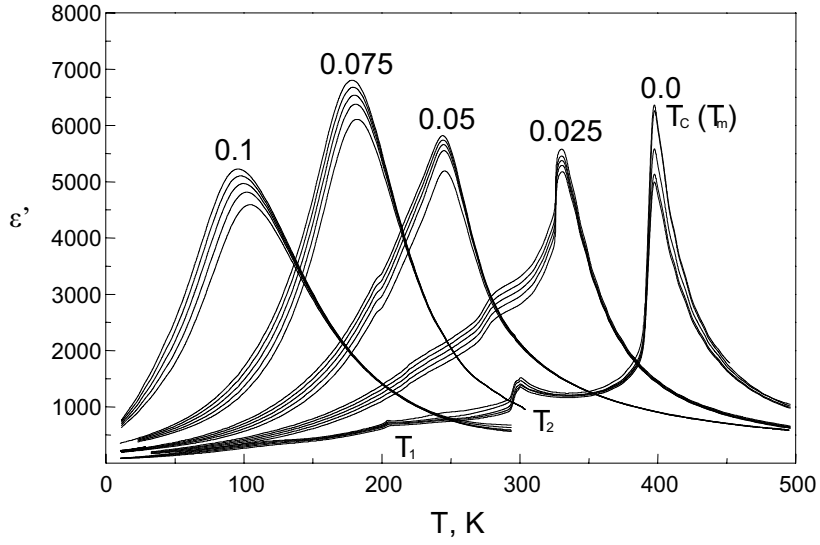

Fig. 1.11. Temperature dependence of the permittivity (real part) of the (1-*x*)$BaTiO_3$ – *x*$La(Mg_{1/2}Ti_{1/2})O_3$ ceramics at 10^2, 10^3, 10^4, 10^5 and 10^6 Hz [53].

The primordial model of Smolensky and Isupov [60] supposes that local fluctuations of the composition result in a distribution of local Curie temperatures, leading to a broadening of the phase transition. Simon *et al.* [52] proposed a model where each substituted atom is assumed to perturb the surrounding host lattice in a finite volume creating a polarized cluster. Such clusters grow at decreasing temperature and reach their maximal size at the Curie temperature T_C. Interaction between these clusters is assumed to be the source of dielectric dispersion. The transformation to relaxor behaviour occurs when the concentration of clusters becomes so large that they cannot reach their maximal size.

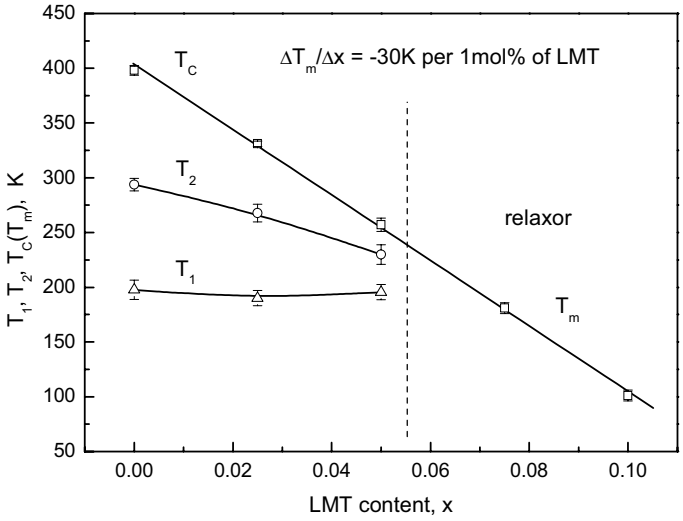

Fig. 1.12. Variation of T_1, T_2 and T_C (T_m) with *x* for ceramics of (1-*x*)BT-*x*LMT at 10^5 Hz [53].

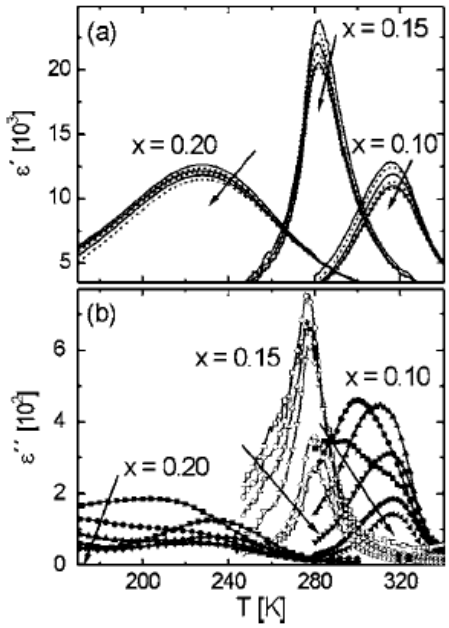

Fig. 1.13. Temperature dependences of the real (a) and imaginary (b) parts of the dielectric permittivity of the $BaTi_{1-x}Sn_xO_3$ ceramics measured at different frequencies, ν =1 Hz–100 kHz [57].

1.6.Bismuth oxide layer structured ferroelectrics

Bismuth-layered ferroelectrics with Aurivillius structure have the general chemical formula $Bi_2A_{n-1}B_nO_{3n+3}$ (n=1–4) and the crystal structure consists of perovskite-like blocks $(A_{n-1}B_nO_{3n+1})^{2-}$ interleaved with fluoride-like $(Bi_2O_2)^{2+}$ layers perpendicular to pseudotetragonal c axis. Here B is a diamagnetic transition metal such as Ti^{4+} or Nb^{5+} and A is an alkali or alkaline earth cation [61].

The important piezoelectric materials with the $(Bi_2O_2)^{2+}$ layer structure (also known as Aurivilius structure) are bismuth titanate ($Bi_4Ti_3O_{12}$) and lead bismuth niobate ($PbBi_2Nb_2O_9$). As shown in Fig. 1.14, the structure of $PbBi_2Nb_4O_9$ consists of corner linked perovskite-like sheets, separated by $(Bi_2O_2)^{2+}$ layers.

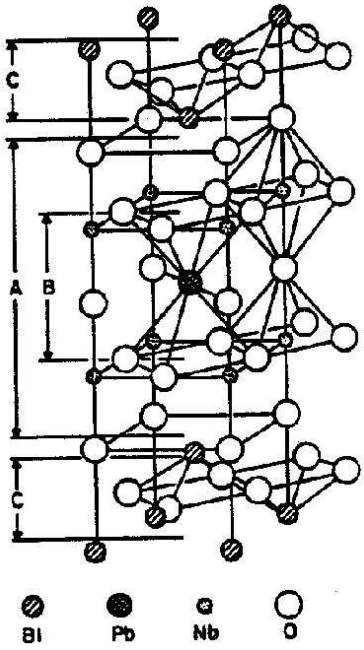

Fig. 1.14. One half of the tetragonal (4/mmm) unit cell of $PbBi_2Nb_2O_9$. A denotes the perovskite double layer $(PbNb_2O_7)^{2-}$; B is a hypothetical $PbNbO_3$ and C denotes the $(Bi_2O_2)^{2+}$ layers [62].

The plate-like crystal structure of these compounds leads to highly anisotropic ferroelectric properties. The ceramics fabricated from the $(Bi_2O_2)^{2+}$ layer compounds do not have very good piezoelectric properties because of a very low poling efficiency. The piezoelectric properties have been shown to be improved by grain orientation during the processing step. One fabrication method involves the tape casting of plate-like $Bi_4Ti_3O_{12}$ and $PbBi_2Nb_4O_9$ powders. The powders get aligned during the formation of the green tape. The orientation is further enhanced on sintering. In the other method, the ceramics is hot forged leading to the orientation of the grains along the forged direction [63,64].

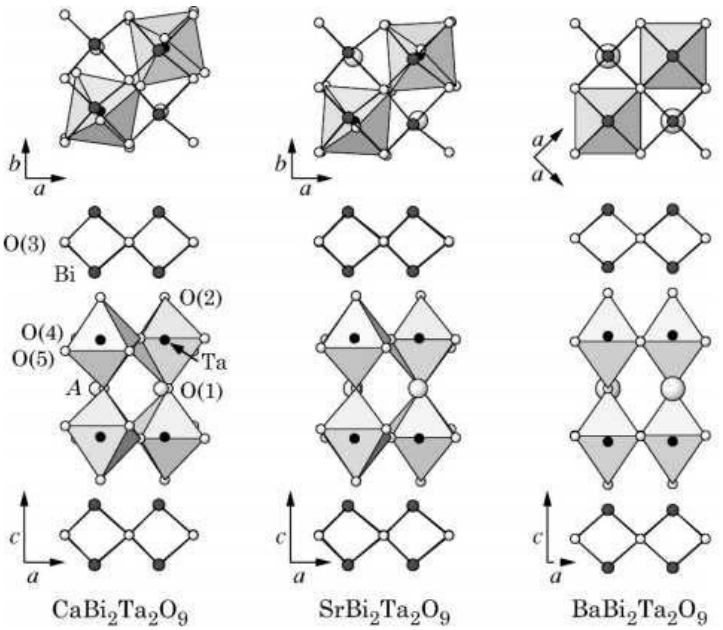

Fig. 1.15. Crystal structures of $ABi_2Ta_2O_9$ (A=Ca,Sr and Ba) drawn with the positional parameters refined with the neutron-diffraction data [65]

Other important Bi-layered materials, first discovered by Smolenskii et al. [66], are Ba-based ferroelectrics $BaBi_2Ta_2O_9$ (BBT), $BaBi_2Nb_2O_9$ (BBN) together with their solid solutions $Ba_{1-x}Sr_xBi_2Ta_2O_9$. The crystal structure of

$SrBi_2Ta_2O_9$ consists of Bi_2O_2 layers and perovskite-type $SrTa_2O_7$ units with double TaO_6 octahedral layers. It was studied by using neutron and electron diffraction, which revealed orthorhombic distortion with space group $A2_1am$ [67]. The structural distortion with this noncentrosymmetric space group is responsible for the displacive-type ferroelectric behaviour of the compound, i.e., atomic displacements along the a axis from corresponding positions in the parent tetragonal ($I4/mmm$) structure cause spontaneous ferroelectric polarization.

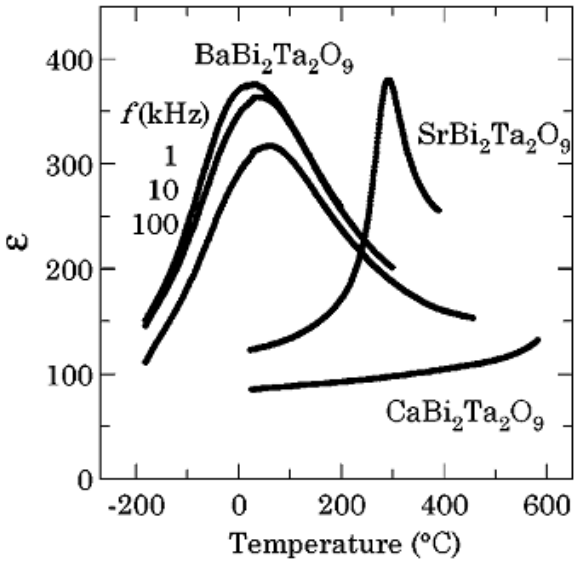

Fig. 1.16. Temperature dependence of the dielectric permittivity of $A$$Bi_2Ta_2O_9$ (A=Ca,Sr and Ba) [65].

The diffraction pattern of $BaBi_2Ta_2O_9$ exhibiting the pseudotetragonal unit cell must reflect the ‘‘averaged’’ structure, i.e., the $BaBi_2Ta_2O_9$ structure consists of microdomains with orthorhombic distortion, which causes the relaxor-type ferroelectric transition (Fig. 1.16) [65]. The anisotropic peak broadening and the large thermal parameters revealed in the structure refinement based on the macroscopic $I4/mmm$ tetragonal symmetry also result from the microscopic structural distortion.

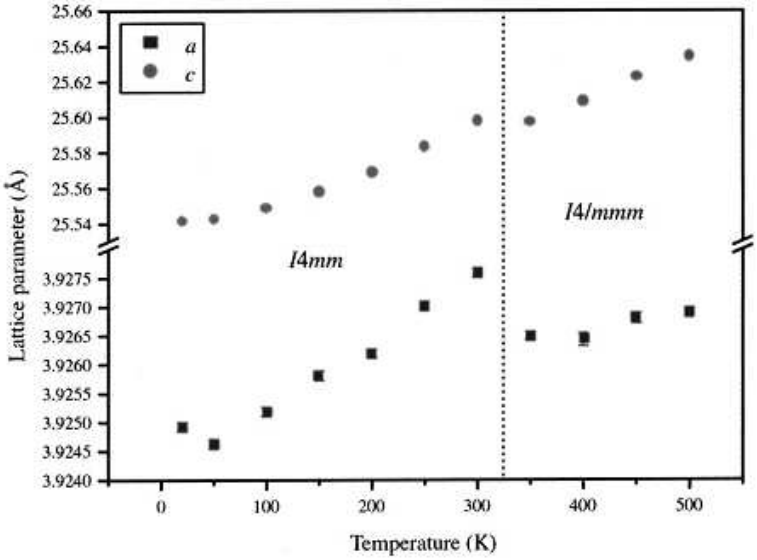

Fig.1.17. Lattice parameters for $BaBi_2Nb_2O_9$ as a function of temperature [68].

The structure studies of $BaBi_2Nb_2O_9$ ceramics [68] suggests the low-temperature ferroelectric structure to be well described in space group *I*4*mm*, while the high-temperature (above 300 K) structure is in the more common *I*4/*mmm* space group, corresponding to the phase transformation at about 320 K.

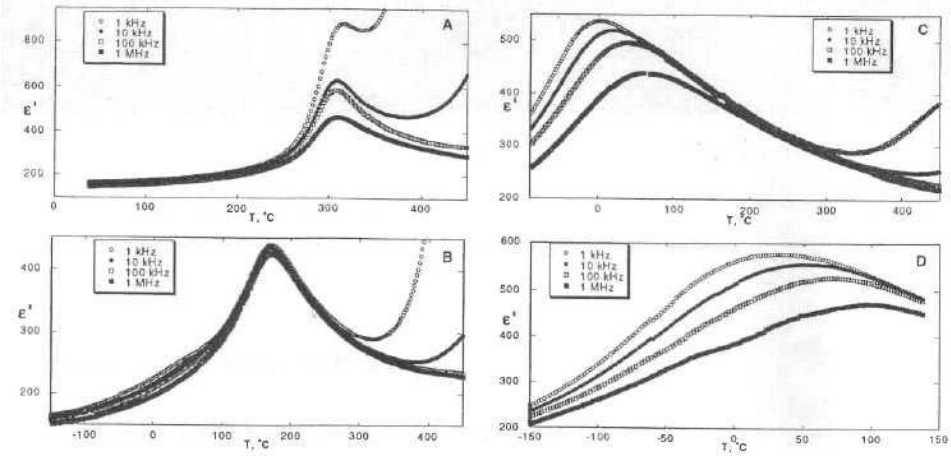

Fig. 1.18. Temperature dependences of ε' for xBBT-(1-x)SBT compositions, x=0 (A), 0.25 (B), 0.75 (C), 1 (D) [69].

Dielectric properties of mixed $SrBi_2Ta_2O_9$ - $BaBi_2Ta_2O_9$ (SBT-BBT) compositions, measured in low-frequency range (Fig. 1.18) shows the ability of $\varepsilon'(T)$ variation as substitution of stroncium in SBT by barium induces the shift of phase transformation temperature to lower values while introducing a frequency dispersion similar to ferroelectric relaxors [69].

The bismuth oxide layer structured ferroelectrics may become important piezoelectric ceramics because of their higher stability, higher operating temperature (T_c = 550-650^{o}C), and higher operating frequency. These ceramics are mainly useful for piezoelectric resonators which need to exhibit a very stable resonant frequency. Although the ferroelectric properties of these oxides have been known for more than 50 years [63,66], most extensive studies have been carried out only during the last 10 years. The increased interest is owing to the high spontaneous polarization, fatigue-free behaviour and low leakage currents of these compounds, which make them promising for applications in nonvolatile ferroelectric memories [70-72]. The most intensively studied are $SrBi_2Ta_2O_9$ (SBT) (n=2) thin films, which are already utilized in FERAMs.

There are still open questions – are the dipolar glasses and relaxors the same, but only different origin – order - disorder type and displacive type? How differ the dynamics of the phase transitions in both cases? The aim of the present work was to try to find answers to these questions using the broadband dielectric spectroscopy.

2. BROADBAND DIELECTRIC SPECTROSCOPY

This chapter includes the methods of the dielectric spectroscopy and measurement technique that was used for the investigation of the relaxor ceramics.

2.1.Low-frequency measurements

In the low-frequency (20 Hz – 1 MHz) range, capacitance C_c and tangent losses $\mathrm{tg}\delta = \varepsilon''/\varepsilon'$ of the sample was measured with the LCR meter HP4284. For all measurements the silver past was used for contacts. Complex dielectric permittivity was calculated from the plane capacitor formulas [73]:

$$\varepsilon' = \frac{(C'_{css} - C_{c0})d}{\varepsilon_0 S_s} + 1, \tag{2.1a}$$

$$tg\delta = \frac{C'_{css} tg\delta_{ss} - C_{c0} tg\delta_0}{C'_{css} - C_{c0}}, \tag{2.1b}$$

where C'_{css} and $tg\delta_{ss}$ are the capacitance and tangent losses of the system with the sample, C_{c0} and $tg\delta_0$ are the capacitance and tangent losses of the system without the sample, d is the height of the sample, S_s is the area of the sample, ε_0 is the dielectric permittivity of vacuum. The area of the sample was much larger as square of the height d^2 so that the field effects were insignificant to all experiments performed. The temperature was measured with copper-constantan thermocouple, which had one stub in the sample and another in the ice and water mixture. Measurements were performed on during continuous temperature variation with typical rate of 1 K/min. All measurements were performed on cooling and heating but most of presented results are on cooling. Home made furnace was used for heating and for cooling was used liquid nitrogen in all experiments.

2.2.High-frequency measurements

The coaxial technique is the most convenient for the dielectric spectroscopy of solids in the 1 MHz – 3 GHz frequency range. The specimen was placed at the end of the coaxial line between the inner conductor and the short piston where it formed a capacitor. Such configuration allowed placing easily the capacitor into temperature-control device. Broadband coaxial lines were used. From the low-frequency end they could be used at any frequency. From the superhigh-frequency end the condition of propagation of the main TEM-wave limits application of the coaxial lines. This condition is given by [73]:

$$\lambda_{00} > \pi(r_3 + r_4), \tag{2.2}$$

where r_3 and r_4 are the radii of the inner and outward conductors of the coaxial line, λ_{00} is the length of electromagnetic waves.

2.3.Experimental details

Most of high-frequency experiments were performed with a coaxial dielectric spectrometer [74]. The core of this coaxial spectrometer was complex reflection coefficient measurement unit P4-11 and vector network analyzer Agilent 8714 ET. The complex reflection coefficient $R^*(v, T)$ was obtained by amplifying the incident and reflected signals by a frequency converter and detected by synchronous amplitude and phase detectors.

Inhomogeneities of the line and distortion in a high-frequency part of the spectrometer (influence of which increases with the increase of frequency) can be taken into account using a computer and digital processing of information by an analysis of the six-port between the capacitor and the output planes of the directional couples. The linear eight-port can be described by a scattering matrix $\|U_{ri}\|$ of the complex coefficients $U_{ri}=b_r/a_i$, relating a reflected signal b_r from the input signal a_i at input i. The indicator of the setup measures the reflection factor R_m (i. e., the ratio of outcoming signals from the measuring and referenced output $R_m=b_3/b_4$).

For an ideal reflectometer setup (R_2=R_3=R_4=0):

$$R_m = \frac{U_{12}U_{31}}{P_{42}} R = o_k R\,, \tag{2.3}$$

where the coefficient o_k can be found by calibrating the spectrometer using a shot with R= -1. In general, one should solve the set of linear equations:

$$\begin{Vmatrix} a_1 \\ a_2 \\ a_3 \\ a_4 \end{Vmatrix} \times \|U\| = \begin{Vmatrix} b_1 \\ b_2 \\ b_3 \\ b_4 \end{Vmatrix} \tag{2.4}$$

which respect to b_1, b_2, b_3, and b_4. Taking into account the fact that $a_1 = R_1 b_1$, $a_3 = R_3 b_3$ and $a_4 = R_4 b_4$, one could find the relation between the measured reflection factor R_m and the reflection coefficient R:

$$R_m^* = \frac{o_{k1} R^* + o_{k2}}{o_{k3} R^* + 1}\,. \tag{2.5}$$

The coefficients o_{k1}, o_{k2} and o_{k3} are composed from products and sums of the elements of the scattering matrix U_{ri} and the reflection factors from the mixers R_3 and R_4. At every frequency they are determined by measuring the reflection R^i_m from the tree calibration samples (from short and open-circuit lines, and from a sample of known permittivity and small loss (TiO_2, $CaTiO_3$). Using Equation (2.5) for every sample, one obtains a set of three complex linear equations, from which one finds the coefficients k_1, k_2 and k_3.

The dielectric spectra are obtained from the results of the measurements of the complex reflection coefficient $R^*(v, T)$ of the TEM-wave in the coaxial line loaded with the sample in the measuring capacitor. From the complex reflection coefficient $R^*(v, T)$ the complex dielectric permittivity $\varepsilon^*(v, T)$ was obtained according to the formulas presented in Section 2.4.

2.4.Complex dielectric permittivity estimation

Complex reflection coefficient R^* is related with the impedance of measuring capacitor Z^*_{ss} and the systems impedance Z_0:

$$R^* = \frac{Z^*_{ss} - Z_0}{Z^*_{ss} + Z_0}. \tag{2.6}$$

For complex capacitance $C_c{}^*$ = C_c '- iC_c'' of the planar capacitor the relation (2.1a) can be generalized in such a form:

$$\varepsilon' - i\varepsilon'' = \frac{d}{\varepsilon_0 S_s}(C'_c - iC''_c) + 1. \tag{2.7}$$

There is a well known relation between the complex impedance Z_{ss} and the complex capacitance $C_c{}^*$:

$$Z_{ss} = \frac{1}{\omega(C'_{css} + iC''_{css})}. \tag{2.8}$$

From Eqs. (2.6), (2.7) and (2.8) we obtain the formulas for the real and imaginary parts of the complex dielectric permittivity ε^*:

$$\varepsilon' = \frac{d}{\varepsilon_0 S_s}\left(\frac{-2R\sin\varphi}{\omega Z_0(1 + 2R\cos\varphi + R^2)} - C_{c0}\right) + 1, \tag{2.9a}$$

$$\varepsilon'' = \frac{d}{\varepsilon_0 S_s}\frac{1 - R^2}{\omega Z_0(1 + 2R\cos\varphi + R^2)}. \tag{2.9b}$$

The fore-cited equations are applied for a quasistatic capacitor in which capacitance is independent of frequency and the electric field in the sample is homogeneous, just as it is when the dimensions of the capacitors are much smaller in comparison to a wavelength λ_{00} of the exciting electric field. However, with the increase of frequency the electric field in the sample become non-homogeneous and is given by:

$$E = A_k J_0[2\pi / \lambda_{00}(\varepsilon_0\mu_0\varepsilon')^{1/2} r], \tag{2.10}$$

where A_k is the constant, depending on the dimensions of the capacitor, r is the distance from the center of a capacitor along the radius, J_0 is the Bessel function of the first kind of zero order, and μ_0 is the vacuum magnetic permittivity. Finding the zeros of the Bessel function, the radii r_1, r_2, r_3, …, where the field between electrodes of the capacitor is equal to zero, can be obtained. The radius r_1 is given by:

$$r_1 \approx \frac{2.405\lambda_{00}}{2\pi(\varepsilon_0\mu_0\varepsilon')^{1/2}}. \tag{2.11}$$

Taking the radius of the sample $r \leq 0.1\ r_1$, one finds the conditions of the quasi-stationary electric field distribution in the capacitor:

$$r \leq \frac{0.24\lambda_{00}}{2\pi(\varepsilon_0\mu_0\varepsilon')^{1/2}}. \tag{2.12}$$

In this case, a dynamic capacitor, which takes into account inhomogeneous distribution of the electric field in the sample, should be used. Consider now the propagation of electromagnetic waves in the capacitor, which is formed by the cylindrical sample, placed at the end of the coaxial line between the inner conductor and short piston. The harmonic field of frequency ω excites the line, and the main monochromatic TEM-wave propagates along the line without variation along the coordinates z and φ. The wave has only the components of the electromagnetic field E_z and H_φ. In the cylindrical system of coordinates, with the center at the axis of the line, the components E_z and H_φ are given by:

$$E_z = -i(2\pi/\lambda_{00})^2\mu_0(\varepsilon'\mu_0)^{1/2}AJ_0[2\pi r/\lambda_{00}(\varepsilon'\mu_0)^{1/2}], \tag{2.13}$$

$$H_\varphi = -(2\pi/\lambda_{00})^2\varepsilon'\mu_0AJ_0'[2\pi r/\lambda_{00}(\varepsilon'\mu_0)^{1/2}], \tag{2.14}$$

where J'_0 is the derivate of the Bessel function J_0.

The impedance of the capacitor under study is given by:

$$Z = \frac{d}{2\pi r}\frac{E_z}{H_\varphi}. \tag{2.15}$$

From the comparison of Eqs. (2.8), (2.13), (2.14) and (2.15) we obtained the capacitance of dynamic capacitor:

$$C_c = \frac{\varepsilon'^{1/2} r J_1(\frac{2\pi}{\lambda_{00}} \varepsilon'^{1/2} r)}{(\frac{2\pi}{\lambda_{00}}) d J_0(\frac{2\pi}{\lambda_{00}} \varepsilon^{1/2} r)}. \qquad (2.16)$$

When the quasi-stationary conditions (2.12) are fulfilled, the relationship (2.16) becomes equal to (2.1).

2.5.Method of thin cylindrical rod in a rectangular waveguide

2.5.1. Microwave reflectivity and transmission measurements

For dielectric measurements in the centimetre and millimetre microwave ranges method of thin cylindrical rod in a rectangular waveguide was used. Moduli of microwave reflection and transmission coeficients were measured with automatic dielectric spectrometer (Fig. 2.1). Using generators (ГКЧ-61 for wave range 8 - 12 GHz and P2-65 for range 26 - 37 GHz) as variable frequency sources, and changing only the waveguide terminanting with a matched load, method under study was applied to measurements of moduli of microwave reflection and transmission coeficients in the frequncy range from 8 GHz to 37 GHz. Bandwith of the range is dependent on microwave oscilator bandwith and waveguide wall width. Power meter Я2Р-70 is used for reflection, transmission and reference power measurements. Coupling between computer and measurements equipment realize the interface BG-01 of prof. A. Brilingas. In the interface unit there are digital analogical converters, which are used to alternate the sweeping frequency of oscillators. Oscillators sweeping frequency dependence on signal level of digital / analog converters $\nu = f(N_{DAC})$ was measured with frequency

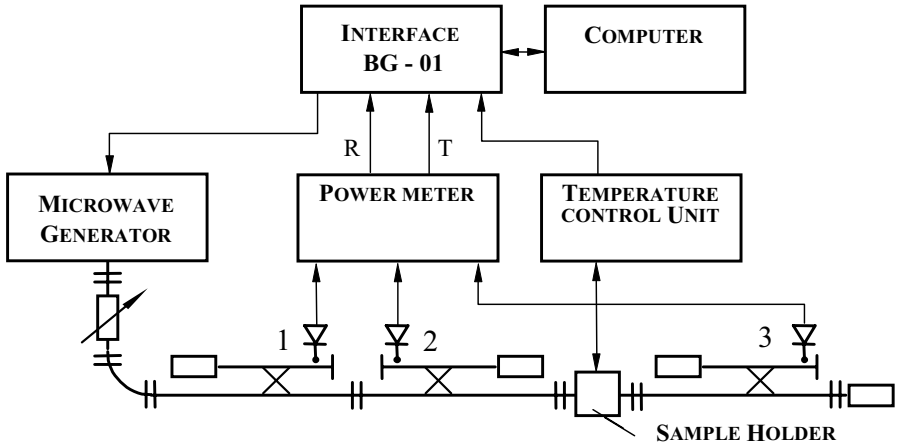

Fig. 2.1. Dielectric spectrometer setup for reflection and transmission measurements in the centimetre and milimetre ranges.

cell and described as a third order polynomial (apart ГКЧ-61, where this function is linear). Frequency measurement errors were less than 0.2% in the centre of the range and 1% in the edges.

Frequency dependencies of reflection R and transmission T_{tr} moduli were measured in all bandwidth of selected range at several hundred points, additionally for each point values was measured on several scan and averaged. Next curves $R=R(\nu)$ and $T_{tr}=T_{tr}(\nu)$ has been sleek, for selected frequencies results was saved in computer. Such processing of results allows to reduce an influence of the random errors and to improve accuracy and plausibility of the method.

The sample of cylindrical shape was placed in the centre of the wide waveguide wall parallel to the electrical field of the main TE_{10} mode. A special sample holder was used. In this sample holder a slot for piston was made. In the piston for sample was made notch, whitch is used for contacts between the sample and a waveguide. Two other pistons were used for calibration of reflections and transmissions. This method allows to reject destruction of waveguide channel, and additionally, allows to verify a calibration during experiment.

2.5.2. Calculation of complex dielectric permittivity

Microwave complex reflection R^* and transmission T^*_{tr} coefficients are dependent on parameters of waveguide system (width of the wall a), frequency of the microwaves, complex dielectric permittivity ε^* and the radius r of a sample. Complex dielectric permittivity $\varepsilon^*(\nu)$ can be estimated from the nonlinear equations $\varepsilon^* = f(R^*)$ or $\varepsilon^* = f(R, T_{tr})$.

A sample of cylindrical form was placed in the centre of the broad wall (or at distance l_0) parallel to the electrical field of the main mode TE_{10} (Fig. 2.2).

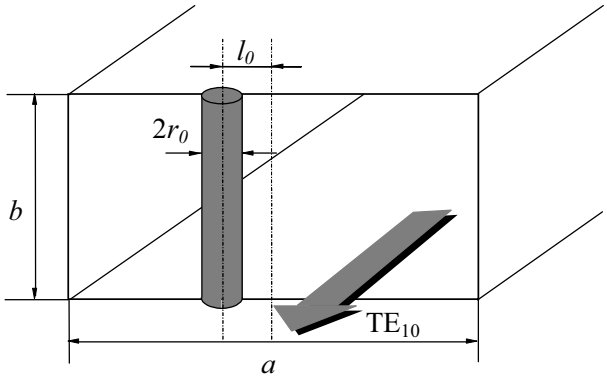

Fig. 2.2. Thin cilindrical rod in a rectangular waveguide.

When a sample is thin enough ($\alpha_0 = 2\pi r/\lambda_{00} \ll 1$), the complex reflection coefficient is [75]:

$$R^* = -\frac{4(\varepsilon^* - 1)J_1(\beta_0)}{\pi\Delta_1\sqrt{\left(\frac{2a}{\lambda_{00}}\right)^2 - 1}}, \qquad (2.17)$$

$$\Delta_1 = \varepsilon^* J_1(\beta_0)\left[H_0^{(2)}(\alpha_0) + 2\sum_{m=1}^{\infty}(-1)^m H_0^{(2)}(2\pi ma/\lambda_{00})\right] - \sqrt{\varepsilon^*}J_0(\beta_0)H_1(\alpha_0),$$

where J_0, J_1 are the Bessel functions, H_1, $H_0^{(2)}$ are the Hankel fuctions, $\beta_0 = k_0(\varepsilon)'^{1/2}r$, a is the width of a waveguide wall.

When a distance from the sample axis to centre of a waveguide wall is l_0, then another expression for complex reflectivity is used [75]:

$$R^* = -\frac{4\sqrt{\varepsilon^*}\cos^2\frac{\pi l_0}{a}}{\pi\sqrt{\left(\frac{2a}{\lambda_{00}}\right)^2 - 1}}\frac{J_1(\beta_0)}{\Delta_2}, \tag{2.18}$$

$$\Delta_2 = -\sqrt{\varepsilon^*}J_0'(\beta_0)\left[H_1^{(2)}(\alpha_0) + 2\sum_{m=1}^{\infty}H_0^{(2)}(2\pi ma/\lambda_{00})\right] - \sum_{m=0}^{\infty}H_0^{(2)}\left[(2m+1)a + 2l_0\right.$$

$$\left. - \sum_{m=0}^{\infty}H_0^{(2)}\left[(2m+1)a - 2l_0\right]2\pi/\lambda_{00} - J_0(\beta_0)H_1^{(2)'}(\alpha_0)\right.$$

For a sample with enough big radius, when condition $\alpha_0 \ll 1$ is not fulfil, more complicated expression for complex reflectivity modulus is used [75]:

$$R^* = -\frac{4(\varepsilon^*-1)}{\pi\sqrt{\left(\frac{2a}{\lambda_{00}}\right)^2 - 1}}\left[\frac{J_1(\beta_0)}{\Delta_1} + \frac{\alpha_0 J_2(\beta_0)}{\Delta_3}\right],$$

$$\Delta_3 = -\sqrt{\varepsilon^*}J_1(\beta_0)\left[H_1^{(2)}(\alpha_0) + \sum_{m=1}^{\infty}\lambda_{00}\frac{(-1)^m}{\pi ma}H_0^{(2)}(2\pi ma/\lambda_{00})\right] + \varepsilon^* J_1'(\beta_0)H_1(\alpha_0).$$

(2.19)

Figs. 2.3 and 2.4 show dependences of $R = R(\varepsilon')$ and $T_{tr} = T_{tr}(\varepsilon')$ for different values of ε''. The best range for determination of ε' and ε'' values is $0.2 < R < 0.85$.

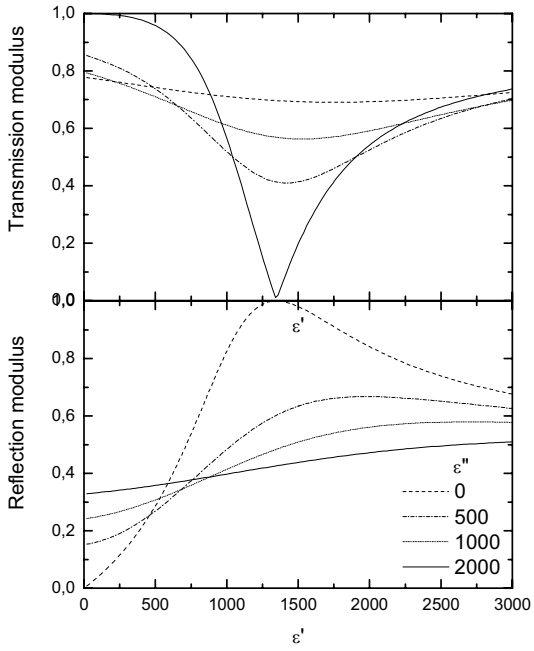

Fig. 2.3. Microwave transmission and reflection coeficients moduli dependence from dielectric permittivity of sample, when ν = 10 GHz, radius of sample r = 100 μm.

When dielectric permittivity is higher, this correction becomes considerable. When losses in the sample are zero then the wave TE_{10} is fully reflected (Fig. 2.3.). This occures for frequency of microwaves:

$$\nu_0 = \frac{c}{2\pi r\sqrt{\varepsilon}}, \tag{2.20}$$

here c is the light velocity in vacuum. When dielectric losses increase, the reflection and transmission coefficients dependence from a real part of dielectric permittivity becomes more shallow. The accuracy of the method decreases, extremely at $\nu > \nu_0$.

For calculating the complex dielectric permittivity the Newton method was used, which allows alternating nonlinear equations system:

$$\begin{aligned} R &= f_1(\varepsilon', \varepsilon'') \\ T_{tr} &= f_2(\varepsilon', \varepsilon'') \end{aligned} \tag{2.21}$$

into linear. The limits of complex dielectric permittivity ε^* and their initial values were chosen aproximately by comparision of high-frequency measurement results. Iteration calculation was stoped, when

$$R - f_1(\varepsilon', \varepsilon'') < \delta_{\text{ac}} \quad \text{and} \quad T_{tr} - f_2(\varepsilon', \varepsilon'') < \delta_{\alpha\chi}; \tag{2.22}$$

there $\delta_{\alpha\chi}$ is the acuracy of calculations. Usualy $\delta_{\alpha\chi}$ is selected around 0,001, calculation with better acuracy is meaningless, because measurements accuracy is less. More information about this method is in [75].

2.5.3. Sample preparation

The method of thin cylindrical rod in rectangular waveguide requeres the samples of cylindrical shape and of height equal to narrow waveguide wall. The samples were prepareted according to measurements methodology requirement, that values of microwave reflection and transmission moduli would be not less then 0.2 and not higher then 0.85. As usual, the samples were cut from big enough piece and further manually polished for desirable dimension was achieved. Shape of the investigated specimens was nearly cilindrical and effective radius r_{ef} was calculated according to formula:

$$r_{ef} = \sqrt{\frac{S}{\pi}}, \tag{2.23}$$

where S is the area of the sample.

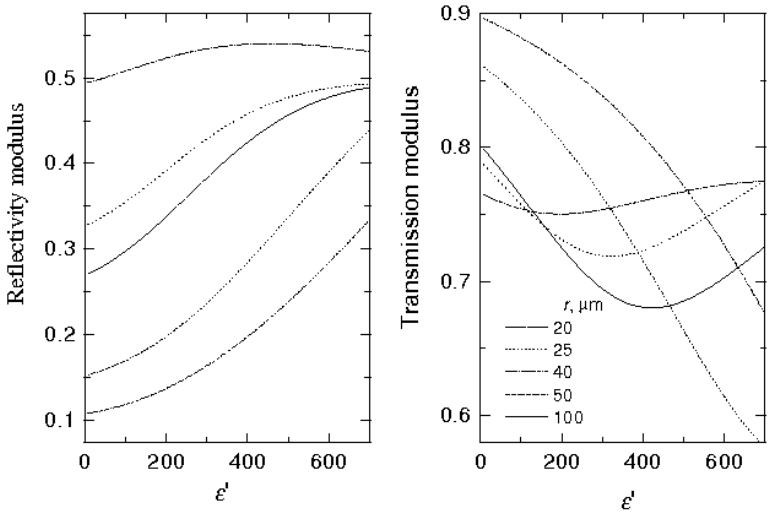

Fig. 2.4 Microwave transmission and reflection coefficients moduli dependence from dielectric permittivity and radius of a sample, when $\nu = 53$ GHz, losses of sample $\varepsilon'' = 400$.

3. BROADBAND DIELECTRIC SPECTROSCOPY OF (1-x)$BaTiO_3$-x$La(Mg_{1/2}Ti_{1/2}O_3)$ FERROELECTRIC RELAXOR CERAMICS

The results of this chapter are published in [P1] and were presented in [C5, C8, C9, C11, C12, C14, C16, C22, C24, C25, C27, C35] scientific conferencies.

(1-x)$BaTiO_3$-x$La(Mg_{1/2}Ti_{1/2}O_3)$ ceramics ((1-*x*)BT-*x*LMT for short) with the compositions x = 0.025 and 0.05 were processed from powders obtained by a chemical route based on the Pechini method, previously optimized for LMT [76]. A stoichiometric mixture of the respective reagent-grade oxides and carbonates was ball-milled in ethanol and calcined at 1470 K for 4 h. Following the latter (chemical) procedure, nitrates of lanthanum and magnesium as well as barium carbonate in proper ratio were dissolved in titanium citrate. The resulting solution was then dried and calcined at 1020 K (2 h) to obtain a fine powder of the desired composition. All the ceramics were sintered in oxygen gas flow at 1720-1770 K for 2-4 hours. Two types of ceramics with x = 0.025 have been obtained. After measurements they were classified into two types: homogeneous one, which showed all three phase transitions of BT type, and non-homogeneous, in which only two phase transitions have been observed. The microstructure was examined by scanning electron microscopy (SEM, Hitachi S-4100) (Fig. 3.1).

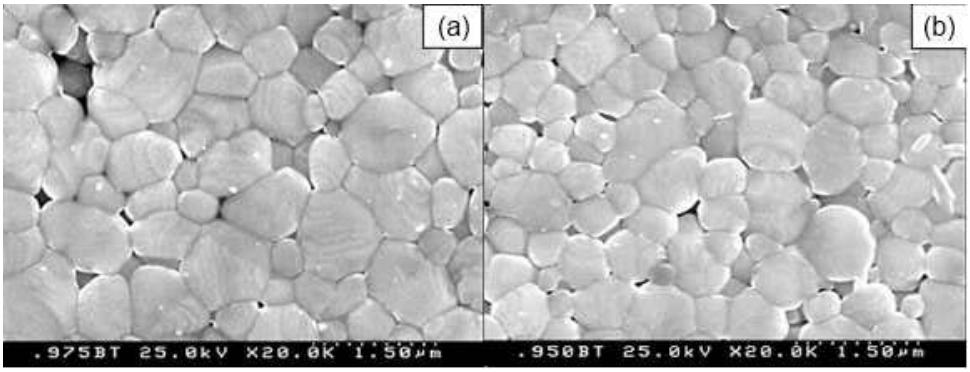

Fig. 3.1. SEM images of polished and thermally etched surfaces of the (1-*x*)BT-*x*LMT ceramics, where *x* = 0.025 (a) and 0.05 (b).

Two types of ceramics of (1-x)$BaTiO_3$-x$La(Mg_{1/2}Ti_{1/2}O_3)$ with x = 0.025 and one with x = 0.05 were dielectrically investigated over the extended frequency range. Dielectric studies have been performed in the frequency range from 20 Hz to 10 GHz within the temperature interval of 100-500 K.

Temperature dependence of the real and imaginary parts of the dielectric permittivity of BT-0.025LMT ceramics are presented in the Fig. 3.2. As it is possible to see, there are three phase transitions as in pure BT. The difference is that these phase transitions are shifted to lower temperatures, compared with BT. Also, below the first phase transition at 320 K, typical relaxor properties are observed. The real part of dielectric permittivity is strongly frequency dependent below 320 K and imaginary part at low frequencies is nearly frequency independent. This is also seen from the frequency dependence of the real and imaginary parts of dielectric permittivity (Fig. 3.3). From the results presented in the Fig. 3.2 and Fig. 3.3, we see, that we have relaxor, which in the low-temperature phase shows another two phase transitions. In the Fig. 3.4 the temperature dependence of the real and imaginary parts of dielectric permittivity of non-homogeneous sample are presented. These temperature dependences differ significantly from the results presented in the Fig.3.2. As we can see, in the temperature dependence of the real part of dielectric

permittivity we can clearly distinguish only two phase transitions: at about 370 K and 300 K. The first one most probably is caused by BT regions, the other one by the rest volume of the ceramics. Due to that we classify this ceramics as non – homogeneous. This ceramics below the phase transition at 300 K shows typical relaxor behaviour as PLZT and other well investigated relaxors [23]. The frequency dependence of the real and imaginary parts of dielectric permittivity of non-homogeneous ceramics confirms typical relaxor behaviour (Fig. 3.5). The real part of the dielectric permittivity shows linear behaviour with frequency, the imaginary part up to microwaves also is frequency nearly independent.

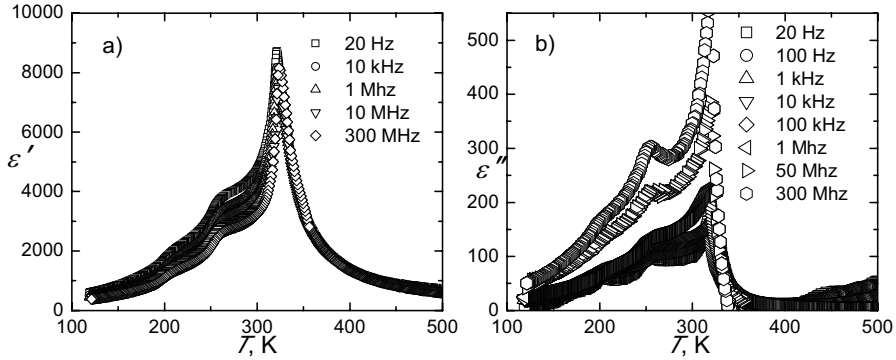

Fig. 3.2. Temperature dependence of the real (a) and imaginary (b) parts of dielectric permittivity at different frequencies of BT-0.025LMT (homogenous).

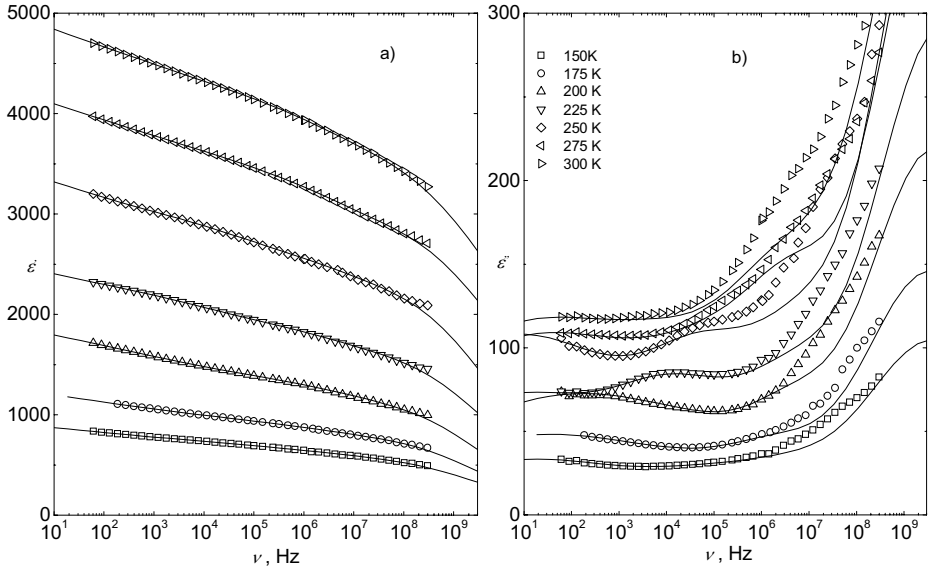

Fig. 3.3. Frequency dependence of the real (a) and imaginary (b) parts of the dielectric permittivity measured in different temperatures. Lines are the best fits with the obtained distribution of the relaxation times (BT-0.025LMT homogenous).

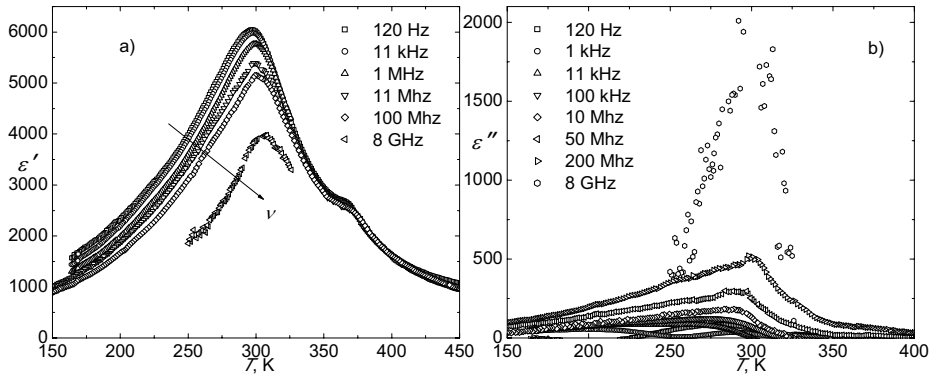

Fig. 3.4. Temperature dependence of the real and imaginary parts of dielectric permittivity at different frequencies of BT-0.025LMT (non-homogenous).

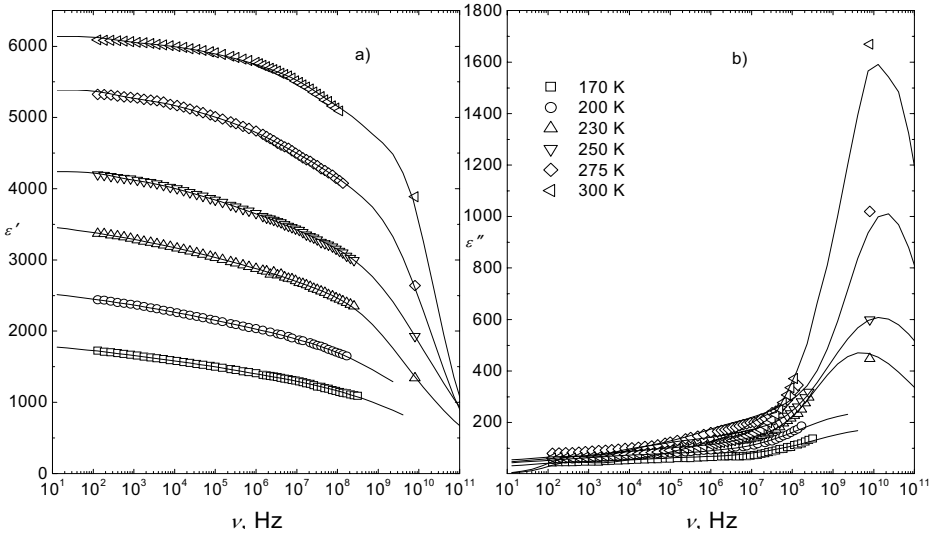

Fig. 3.5. Frequency dependences of the real (a) and imaginary (b) parts of the dielectric permittivity measured in different temperatures. Lines are the best fits with the obtained distribution of the relaxation times (BT-0.025LMT non-homogenous).

Usual evaluation of the dielectric dispersion parameters is performed with Cole – Cole or Havriliak – Negami formulas. Unfortunately, these formulas have defined shape of the distribution of the relaxation time function. As we can see from the Figs 3.3 and 3.5, in our case we have extremely broad and non symmetrical shape of the frequency dependence of the imaginary part of the dielectric permittivity. Also, after careful examination of the frequency dependence of the imaginary part we can see that there are at least two maxima, so there is no possibility to describe dispersion with single Cole - Cole or Havriliak – Negami process (Fig.3.3). In such case we need a new approach to extract the real distribution of the relaxation times from the dielectric spectra. In this study, from the frequency dependence of the real and imaginary parts of dielectric permittivity the distribution of relaxation times is treated as the ensemble of independent Debye-like processes:

$$\varepsilon'(f) = \varepsilon_\infty + \int_{-\infty}^{\infty} \frac{g(\tau)}{1+(2\pi f\tau)^2} d(\ln\tau) \ , \tag{3.1}$$

$$\varepsilon''(f) = \int_{-\infty}^{\infty} \frac{2\pi f\tau g(\tau)}{1+(2\pi f\tau)^2} d(\ln\tau) \ . \tag{3.2}$$

These integral equations have been numerically solved. The Tikhonov regularization method has been used. This method and calculation technique is described in detail elsewhere [77].

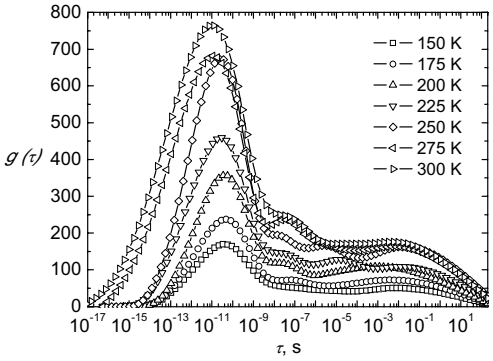

Fig. 3.6. Distribution of the relaxation times of BT-0.025LMT (homogenous).

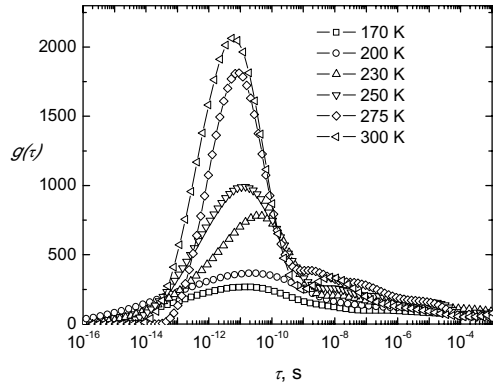

Fig. 3.7. Distribution of the relaxation times of BT-0.025LMT (non-homogenous).

Obtained results are presented in the Figs 3.6 and 3.7. As we see, the distributions of the relaxation times for homogeneous and non–homogeneous ceramics are clearly different. In the case of homogeneous ceramics we observe one maximum at about 10^{-11} s and the broad maximum at longer relaxation times. Similar picture was already obtained for PMN-PSN-PZN relaxor ceramics [23]. With decreasing temperature, the maximum at 10^{-10} s decreases, and becomes comparable with the long relaxation times broad maximum. We assume, that this maximum at about 10^{-11} s is caused by non-polar matrix of relaxor and the long relaxation times and the broad maximum is caused by polar nanoregions, which contribution increases with decreasing temperature. The main difference in comparison with previous results for relaxors is that the long relaxation time edge do not diverge according to Vogel – Fulcher law, but stays nearly constant at all temperatures at about 10 s. Such behaviour can be caused by the limits of our experimental frequency range.

The distribution of the relaxation times for non-homogeneous ceramics (Fig. 3.7) is different. As we can see, we do not observe clearly expressed long relaxation times maximum, instead the maxima of nonpolar matrix decreases with temperature and broadens. This result confirms non homogeneous distribution of LMT in the sample – it does not behave as typical relaxor. It reminds a ferroelectric phase transition, but with a broad distribution of the relaxation times.

The distribution of the relaxation times of BT-LMT ceramics is more similar to the relaxor type, but the dynamics of polar nanoregions is different – no Vogel – Fulcher law dependence of the long relaxation times has been observed. This can be caused by influence of the ferroelectric phase transition at 320 K. Due to that, the dynamics of relaxor-type polar nanoregions is strongly influenced by ferroelectric order, and these regions, caused by substitution of LMT do not give the main contribution to the dielectric permittivity and the dynamics of these regions is completely different from the relaxors.

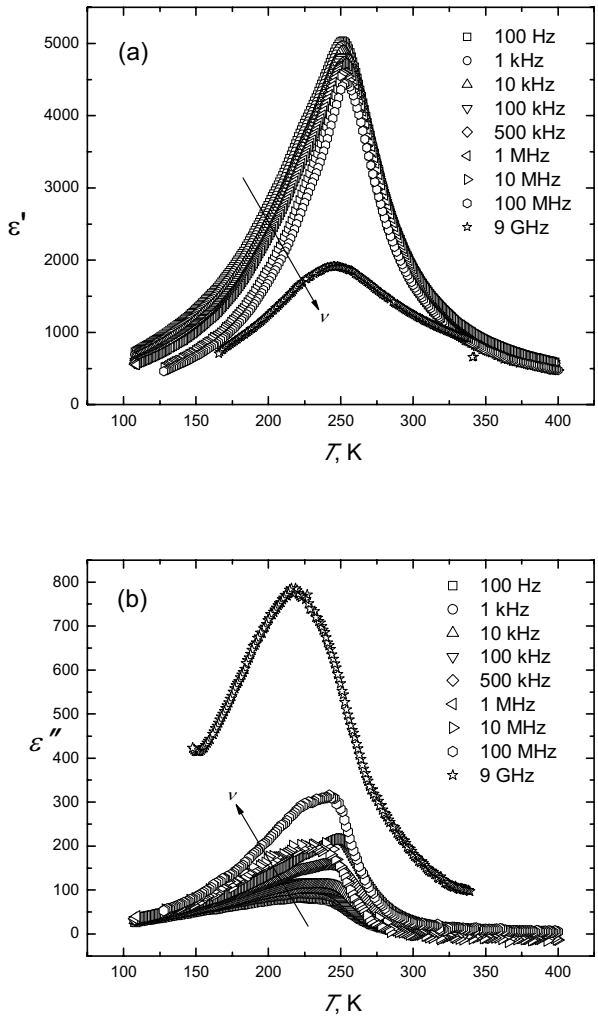

Fig. 3.8. Temperature dependence of the real (a) and imaginary (b) parts of dielectric permittivity at different frequencies of BT-0.05LMT.

But the temperature and frequency dependences look very similar to the relaxor ones. They even look more similar for the relaxor-type for non-homogeneous sample. But after examination of the distribution of the relaxation times (Fig. 3.7) we see, that this ceramics is even more different from relaxors.

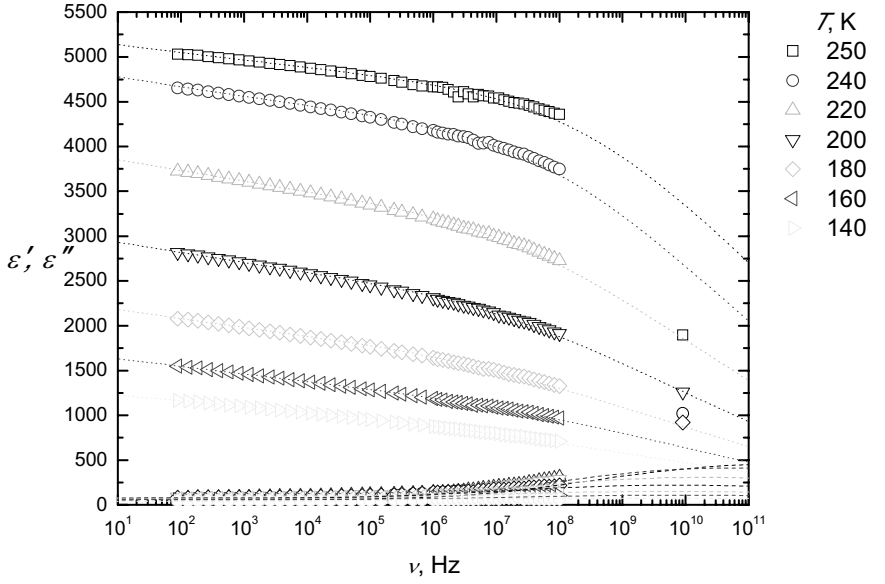

Fig. 3.9. Frequency dependence of the real and imaginary parts of the dielectric permittivity at different temperatures of BT-0.05LMT.

We see, that the main maxima of the distribution of the relaxation times only slightly shifts with temperature and significantly broadens, but we do not observe splitting of the distribution times caused by polar nanoregions.

For ceramics of higher LMT content x = 0.05 (BT-0.05 LMT) only one phase transition, coresponding to the transition from paraelectric to ferroelectric phase in pure $BaTiO_3$ is clearly seen (Fig. 3.8). The transition temperature is about 250 K and it is shifted lower temperatures compared to pure BT (400 K) and BT-0.025 LMT (325 K). The transition is diffused and in temperatures below it showing relaxor-type dispersion, although the maximum value of the dielectric permittivity doesn't have such obvious dependence on frequency as it is obtained for "classical" relaxor materials as PMN.

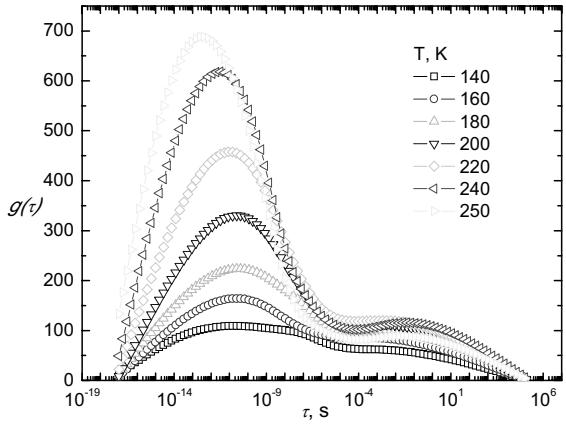

Fig. 3.10. Distribution of the relaxation times of BT-0.05LMT.

The dielectric permittivity from the lowest measured frequencies up to 10^8 Hz is showing nearly linear character, typical for relaxors, and then dramatically reduces at GHz frequencies (Fig. 3.9) – very similar as for BT-0.025 LMT material. The relaxation times have peak at about 10^{-11} – 10^{-12} s with a low decreasing at higher temperatures (Fig. 3.10). The same as for the composition with $x = 0.025$, the long relaxation time edge obviously does not diverge according to Vogel – Fulcher law and that is the main difference from the relaxor behaviour.

From these results we can conclude, that both measured compositions of (1-x)$BaTiO_3$-x$La(Mg_{1/2}Ti_{1/2}O_3)$ family – the one with $x = 0.025$ and $x = 0.05$ show ferroelectric and nearly relaxor properties. We have bridging materials between ferroelectrics and relaxors.

4. DIELECTRIC PROPERTIES OF $BaTi_{(1-x)}Sn_{(x)}O_3$ CERAMICS

Results of this chapter are published in [P7] and were presented in [C18, C26, C28] scientific conferencies.

The $BaTiO_3$ is the classic ferroelectric crystal which was one of the most investigated ferroelectric materials during the years [44,45,47,49,50]. The recent investigations showed that small amount of admixtures changes the nature of the phase transition from ferroelectric to relaxor one. The aim of the present work was to investigate the nature of the relaxor behaviour in isovalently substituted solid solutions $BaTi_{1-x}Sn_xO_3$.

The gradual crossover from ferroelectric to relaxor behaviour is characterized by vanishing of the contribution due to domain walls and appearance of relaxation related to reorientation of polar nanosized regions. Typical behaviour of relaxors is observed only in ceramics with $x = 0.30$, while the compositions with $0.175 \leq x \leq 0.25$ show coexistence of both ferroelectric and relaxor features. The relaxor properties are supposed to be due both to weak random fields and to disorder inherent in pure $BaTiO_3$.

Typically, the relaxor behaviour is observed in compositions with a charge disorder, where cations with different valence randomly occupy equivalent crystallographic positions. Such charge disorder is a source of quenched electric random fields (RFs), which prevent the formation of a long-range ordered ground state in ferroics with continuous symmetry of order parameter. Statistical fluctuations of RFs promote nucleation of PNRs at high temperatures in the paraelectric state. At high temperatures, PNRs have the size of several nanometers and are highly dynamic. This state is called the ergodic relaxor state, since interactions between PNRs are supposed to be weak and the system quickly goes back to the initial state after some excitation. On cooling both a growth of individual PNRs and an increase of their number take place. As a result interactions between PNRs become stronger and finally at a

certain temperature a transition into a short-range ordered glass-like (non-ergodic relaxor) or into a long-range ordered ferroelectric state occurs.

$BaTi_{1-x}Sn_xO_3$ ceramics with x = 0.1 (BTSn10) also was investigated by the broadband dielectric spectroscopy.

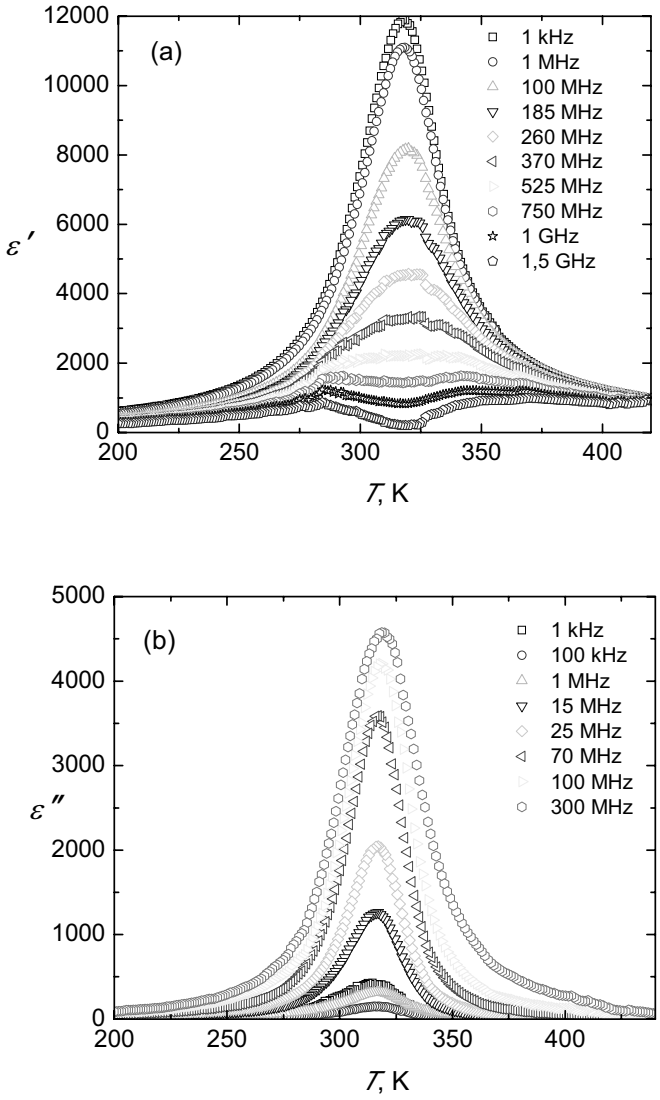

Fig. 4.1. Temperature dependence of the real (a) and imaginary (b) parts of dielectric permittivity at different frequencies of BTSn10 ceramics.

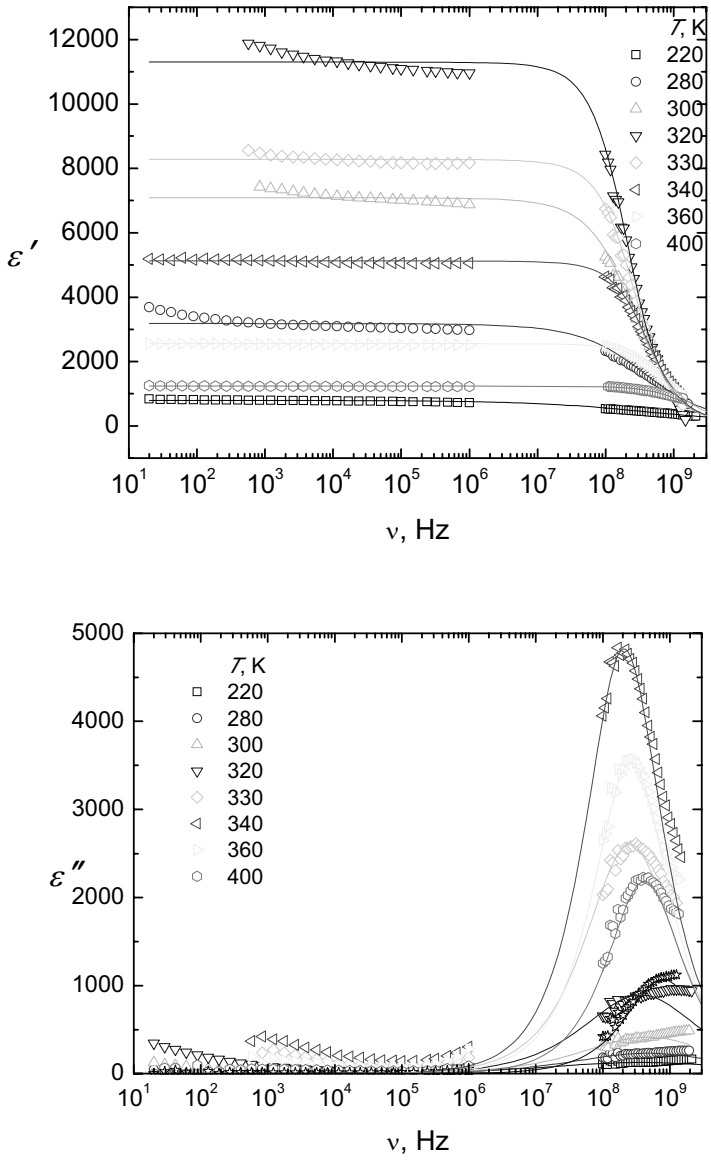

Fig. 4.2. Frequency dependence of the real (a) and imaginary (b) parts of the dielectric permittivity of BTSn10 measured in different temperatures. Lines are the best fits with the obtained distribution of the relaxation times.

We can see huge dielectric dispersion in both higher and lower temperatures around the phase transition (Fig. 4.1). The temperature of the phase transition (320 K) is shifted to lower temperatures compared to that of pure BT. The dispersion character is obviously non relaxor-type.

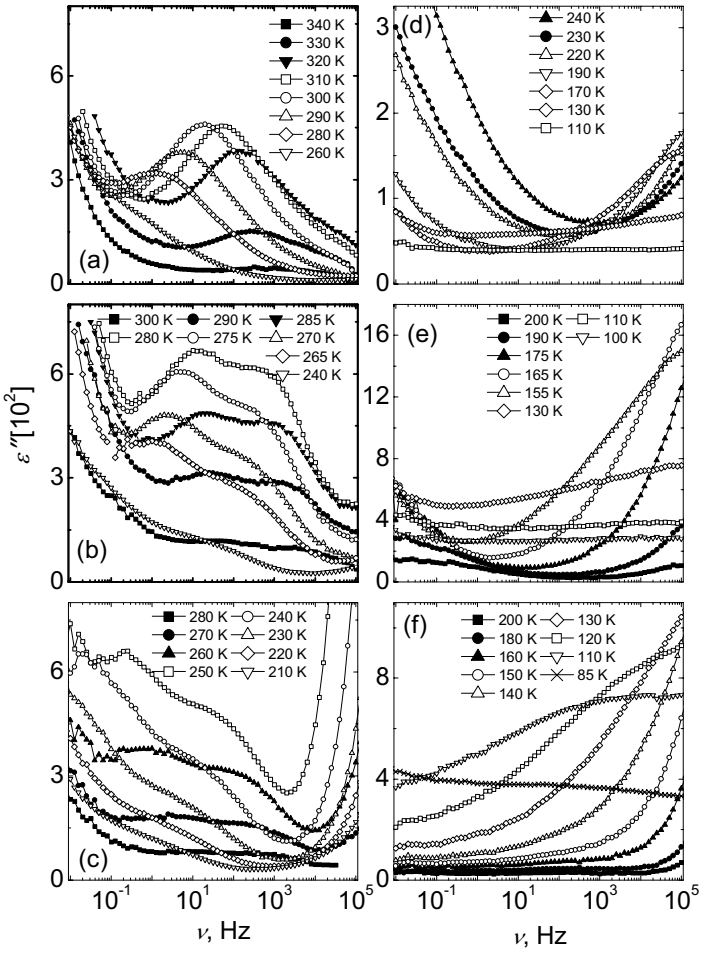

Fig. 4.3. Frequency dependence of the imaginary part of the dielectric permittivity of $BaTi_{1-x}Sn_xO_3$ ceramics with x=0.10 (a), 0.15 (b), 0.175 (c), 0.20 (d), 0.25 (e), and 0.30 (f), all measured in the frequency range 10^{-2}–10^5 Hz. In all graphs the solid and open symbols correspond to temperatures above and below T_m (ν = 100 kHz), respectively.

It was supposed [57] that PNRs in BTSn ceramic appear only above a certain doping level, when the effects of random fields become substantial. Recently, however, we found that even in BTSn10 a high-frequency relaxation is already observed above T_m at frequencies 108–109 Hz (Fig. 4.2). A similar relaxation starting above T_m was observed also in pure $BaTiO_3$ [78]. It was related to a hopping of the off-center Ti^{4+} cations between symmetry-related potential wells, pointing out that the phase transition in $BaTiO_3$ rather follows an order–disorder scenario than a purely displacive one.

The measurements in low frequency range were performed in cooperation with Duisburg University (Germany). Ceramics with x=0.15, 0.175, 0.2, 0.25 and 0.3 were measured down to 10^{-2} Hz (Fig. 4.3).

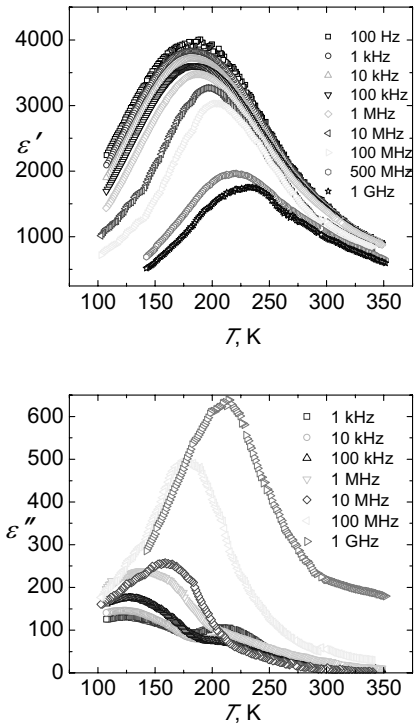

Fig. 4.4. Temperature dependence of the real (a) and imaginary (b) parts of dielectric permittivity at different frequencies of BTSn25 ceramics.

The transformation to relaxor behaviour in BTSn is supposed to be related to the disorder within the B-sites of the perovskite-type ABO_3 unit cell. Indeed, the ferroelectricity in barium titanate resides on a cooperative shift of Ti^{4+} cation into a certain direction from the center of the oxygen octahedron. The larger tin cation cannot shift off-center, giving rise to random breaking of the correlated displacement along Ti-O-Ti-O chains. As the tin content increases (Figs. 4.4 and 4.5), the regions with an accumulated concentration of broken bonds will occupy a larger part of the sample. As a consequence, the polar correlations are strongly diminished and ferroelectric domains are less likely to nucleate. However, due to the distortions arising around the tin ions a redistribution of the charges and a local formation of charged centers results. These are sources of local random fields, whose quenched spatial fluctuations act as pinning centers of the thermally fluctuating polarization.

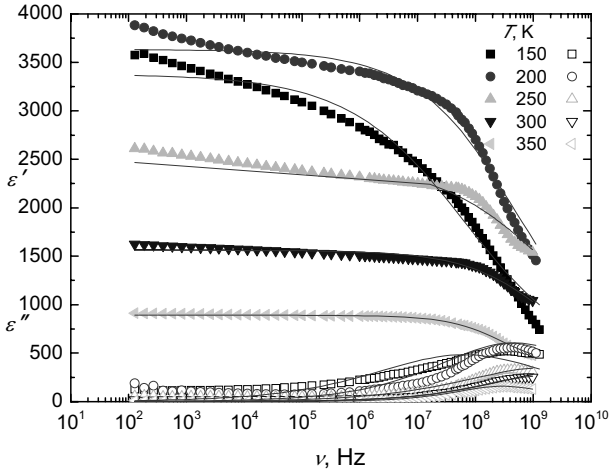

Fig. 4.5. Frequency dependence of the real and imaginary parts of the dielectric permittivity at different temperatures of BTSn25 ceramics.

Clearly, this kind of random fields is much weaker than that resulting from heterovalent cation substitution as in conventional relaxors. Hence, the relaxor properties of BTSn require relatively high doping.

The following conclusions have been made from the above results. Dielectric spectroscopical data evidence a ferroelectric state in compositions with $x < 0.175$ (Fig. 4.3). Relaxor-type relaxations related to the reorientation of PNRs appear in compositions with higher tin content. However, the phase transitions in ceramics with $x = 0.20$ and 0.25 occur at higher temperatures than the freezing of PNRs dynamics. Only in BTSn30 the relaxor-type transition into a glass-like state takes place. The relaxor properties in BTSn are supposed to be induced by weak random fields. On the other hand, dynamic superparaelectric moments that also exist in the pure barium titanate are proposed to be precursors of PNRs in related solid solutions.

5. DIELECTRIC PROPERTIES OF $Ba_{1-x}Sr_xBi_2Ta_2O_9$ CERAMICS

The results of this chapter are published in [P4] and [P5] and were presented in [C3, C4, C7, C10, C13, C17, C20, and C29] scientific conferences.

The $Ba_{1-x}Sr_xBi_2Ta_2O_9$ (alternatively marked as (x)BBT-(1-x)SBT) solid solutions possess Bi-layered Aurivilius structure, which was portrayed in Chapter 1.6. SBT composition (x = 0) presents a typical ferroelectric behaviour with a phase transition occurring at ~320°C. As for BBT (x = 1), it exhibits a ferroelectric relaxor behaviour; a diffuse phase transition is observed at lower temperatures and its dielectric curve exhibits a strong relaxation in the studied frequency range where its maximum of permittivity T_m shifts to higher temperature as the frequency increases. It is commonly accepted that, when strontium is substituted by barium, a significant positional disorder is induced in SBT which is considered to be the main cause of the broadening of the phase transition in BBT. Substituting small amounts of strontium by barium, a shift of the Curie temperature towards lower values is observed while a frequency dispersion of the permittivity values at lower temperatures appears. This effect is already visible for x = 0.25. As x increases, the maximum of permittivity keeps moving to lower temperatures approaching the temperature region where diffuse phase transition in BBT is observed.

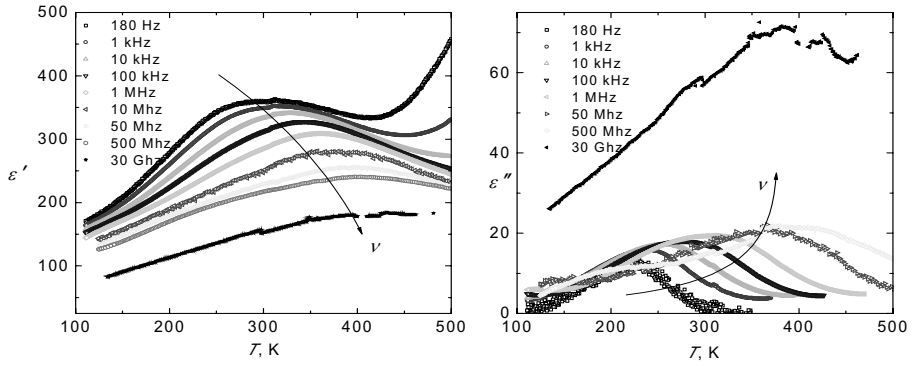

Fig. 5.1. Temperature dependence of the real and imaginary parts of the dielectric permittivity measured in different frequencies for BBT ceramics.

Figure 5.1 shows the real and imaginary parts of dielectric permittivity temperature dependence at different frequencies. As it possible to see, the maximum value of dielectric permittivity reaches only 370 at low frequencies.

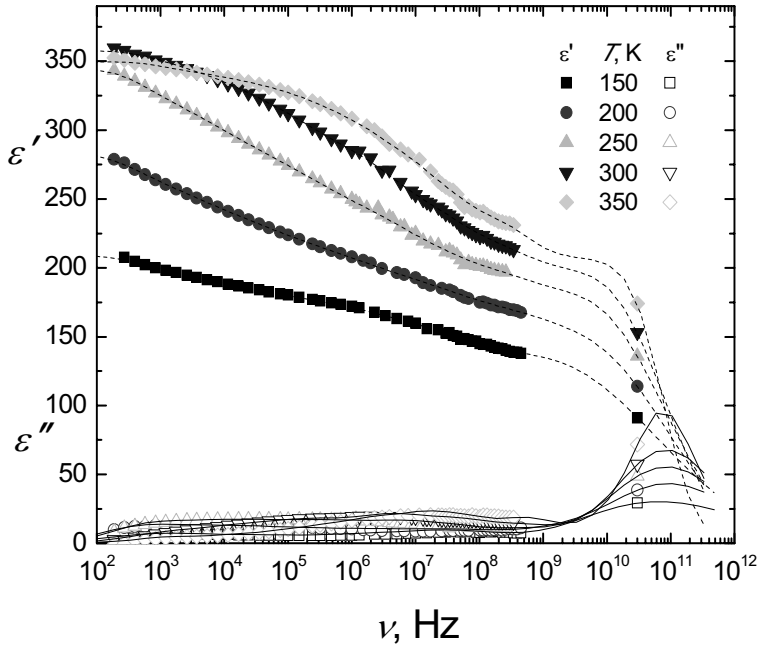

Fig. 5.2. Frequency dependence of the real and imaginary parts of the dielectric permittivity of BBT measured in different temperatures.

Such low value is not typical for relaxors. For lead containing relaxors it is of order 10000 or higher [21]. But the frequency – temperature behaviour is typical for relaxors: maximum of the real part of dielectric permittivity shifts to higher temperatures with increase of the frequency. Imaginary part also behaves very typically as for relaxors. Such low value of dielectric permittivity is probably related to reduced polarizability of the host ions and weak interaction between the dipole moments [79]. It should be mentioned, that maxima of the real part of dielectric permittivity shifts much stronger to higher temperatures with increasing frequency as in lead containing relaxors, such as

PLZT [21]. We must mark that at high temperatures and low frequencies conductivity contribution was observed (Fig.5.1).

Frequency dependencies of the real and imaginary parts of dielectric permittivity are presented in Fig. 5.2. The dielectric dispersion clearly appears at low temperatures and extends to the microwave region. A less pronounced dispersion of dielectric permittivity can be seen even at low temperatures. In contrast to the classical relaxors, this dispersion region is temperature dependent and shifts to the lower frequency region with decreasing temperature and we do not observe flat dependence of the imaginary part of the dielectric permittivity, but the real part of dielectric permittivity at low temperatures behaves nearly linearly as it should be for relaxors.

At low temperatures it is possible to see two maxima in the frequency dependence of the imaginary part of dielectric permittivity. Low-frequency maxima (clearly seen in the Fig. 5.2 at 10^3 Hz at 150 K) most probably is related to polar nanoregions dynamics, and high-frequency maxima (at 150 K) is caused by nonpolar matrix of ceramics.

Due to pronounced dispersion even at low frequencies we have used usual Cole – Cole model to obtain dispersion parameters:

$$\varepsilon^* = \varepsilon_\infty + \frac{\Delta\varepsilon}{1+(i\omega\tau)^{1-\alpha}} . \qquad (5.1)$$

In this equation $\Delta\varepsilon$ represents the strength of relaxator, τ is the mean Cole - Cole relaxation time, α is the relaxation time distribution parameter, ε_∞ is the contribution of all phonon modes and electronic polarization. Calculated Cole - Cole dielectric dispersion parameters are presented in the Fig. 5.3. The parameter of the distribution of relaxation times α has values of 0.8 - 0.9 in the whole temperature range. This means that the distribution of relaxation times is extremely broad.

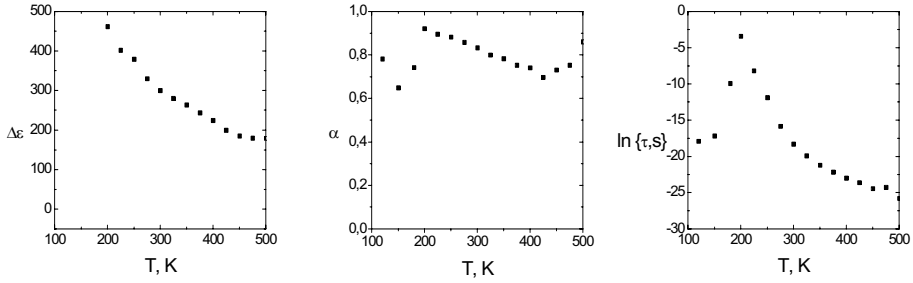

Fig. 5.3. Cole – Cole fit parameters $\Delta\varepsilon$, α, τ.

The mean Cole - Cole relaxation time of present ceramic diverges with temperature according to Vogel - Fulcher law:

$$\tau = \tau_0 e^{\frac{E}{k(T-T_0)}} \tag{5.2}$$

The Vogel - Fulcher fit (Fig. 5.4) parameters are: $\tau_0 = 2.34 \cdot 10^{-14}$ s, $T_0 = 92$ K, $E/k_b = 3302$ K. Parameters of the dielectric dispersion are presented in the Fig.5.3. Such behaviour of the relaxation time temperature dependence is caused by complicated dynamics: splitting of the maxima of imaginary part of dielectric permittivity into two peaks, but the fits where performed with single Cole – Cole process. Also the distribution parameter alpha reaches very high value in the whole investigated temperature range.

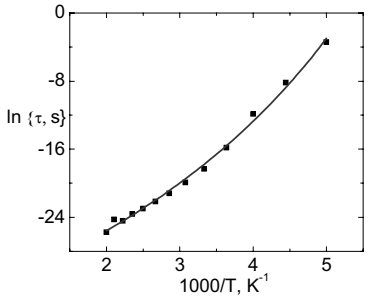

Fig. 5.4. Relaxation time fit with Vogel – Fulcher law.

However, at low temperatures the behaviour of dielectric permittivity (ε" in low frequencies is almost frequency independent, having a peak at ≈ 10^{11} Hz; the dielectric spectrum is very diffused) suggests that Cole - Cole approximation is not the best choice due to unsymmetrical shape of the distribution of relaxation times.

The relaxation time distribution function at different temperatures was calculated according to the following procedure. The original program performs the direct calculation of the relaxation time distribution function $f(\tau)$ from the frequency dependence of the complex dielectric permittivity at fixed temperatures according to superposition of Debye-like processes (for details see [77]).

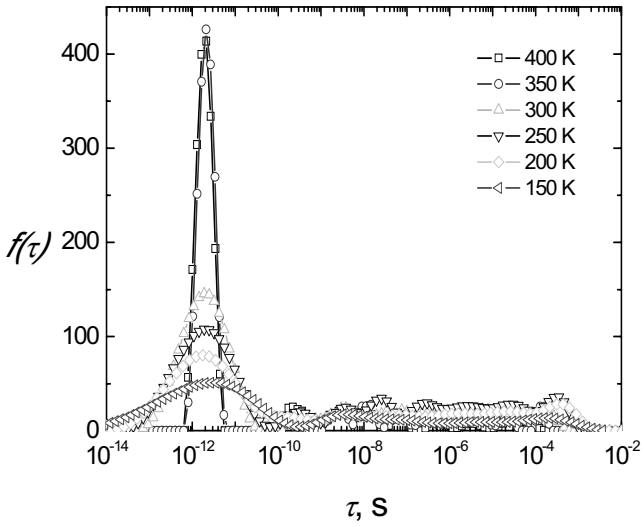

Fig. 5.5. Relaxation time distribution function *f(t)* of BBT ceramics at different temperatures.

The real distribution function of the relaxation times of BBT ceramics (Fig. 5.5) was calculated from the dielectric measurements results. Relaxation times scatter over the interval of 10^{-15} – 10^{-2} s. With the increase of the temperature

the *f(t)* function peak, responding to the $2 \bullet 10^{-12}$ s time of relaxation, increases and reaches the biggest value at 350 K.

As the main attention was focused on BBT material (x = 1), but the dielectric measurements were also made for other materials with x = 0.25, 0.5 and 0.75, we present here only brief review and the main graphs of the dielectric spectra for these ceramics. For xBBT-(1-x)SBT solid solution with x = 0.25, obtained results are presented in Figs. 5.6 - 5.8, for x = 0.5 in Figs. 5.9 – 5.10 and for x = 0.75 in Fig. 5.11. The dielectric dispersion in these ceramics with x = 0.25, 0.5 and 0.75 is not typical nor for ferroelectrics, nor ferroelectric relaxors. In the whole frequency range, even at lower temperatures we observe maxima in imaginary part of dielectric permittivity. Such behaviour is more similar to dipolar glasses than to relaxors. The distribution of relaxation times (Fig. 5.8) shows the existence of at least two-component behaviour – the spherical glassy matrix and the ferroelectric clusters. These clusters (polar nanoregions) are present and make noticeable influence to the dielectric permittivity of xBBT-(1-x)SBT solid solutions at temperatures below a phase transition.

x = 0.25

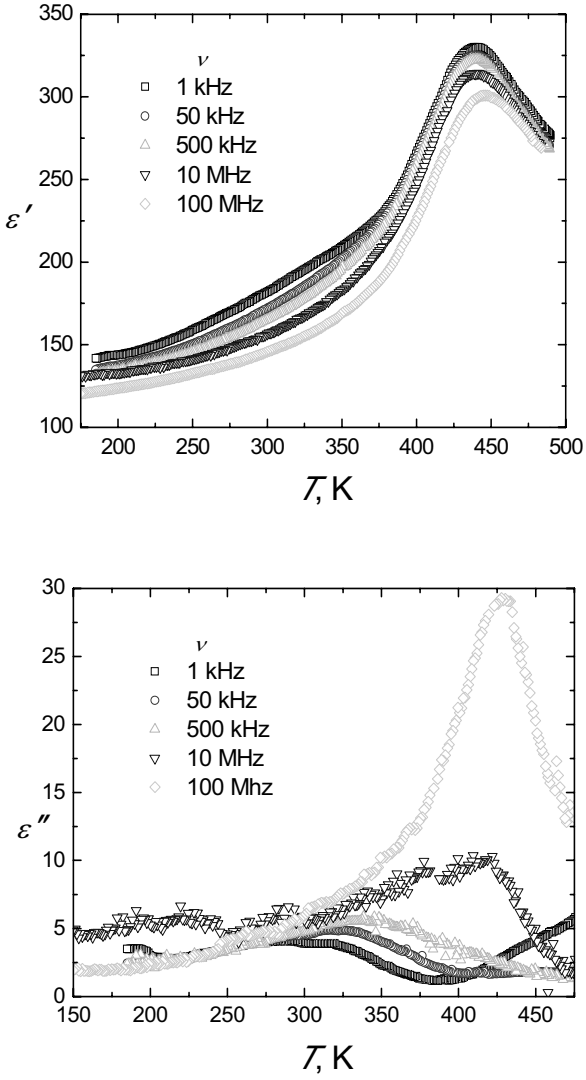

Fig. 5.6. Temperature dependence of the real (a) and imaginary (b) parts of the dielectric permittivity of 0.25BBT-0.75SBT ceramics, measured in different frequencies.

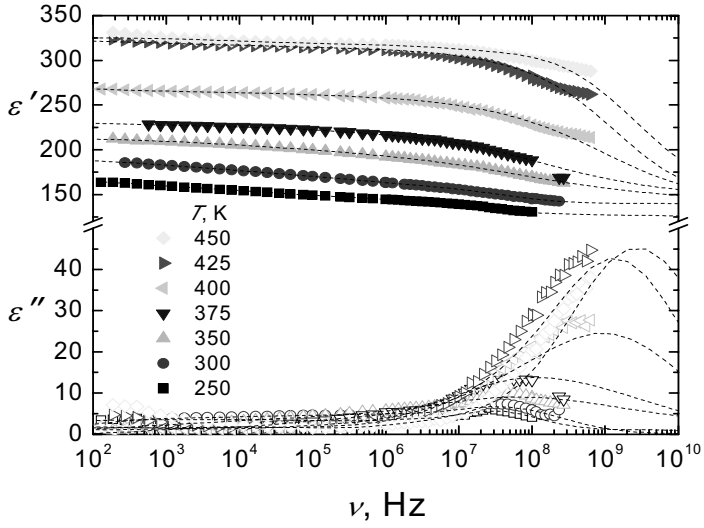

Fig. 5.7. Frequency dependence of the real and imaginary parts of the dielectric permittivity of 0.25BBT-0.75SBT measured in different temperatures.

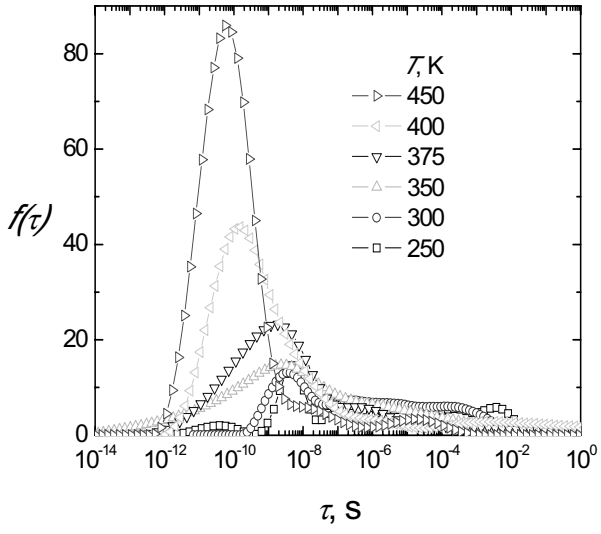

Fig. 5.8. Relaxation time distribution function *f(t)* of 0.25BBT-0.75SBT ceramics at different temperatures.

x = 0.5

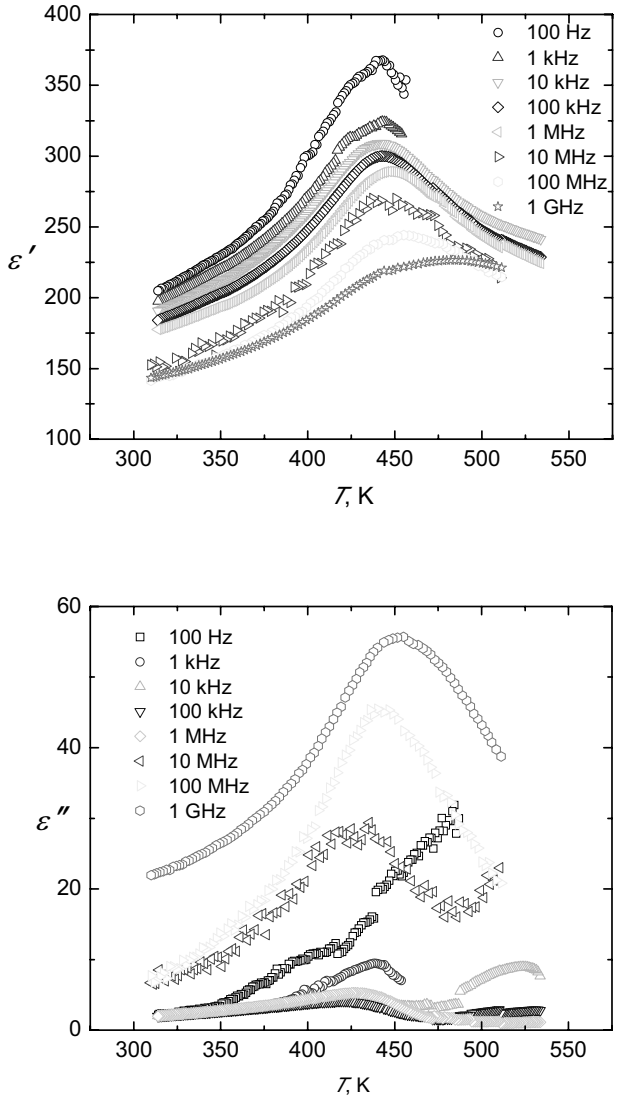

Fig. 5.9. Temperature dependence of the real (a) and imaginary (b) parts of the dielectric permittivity of 0.5BBT-0.5SBT ceramics, measured in different frequencies.

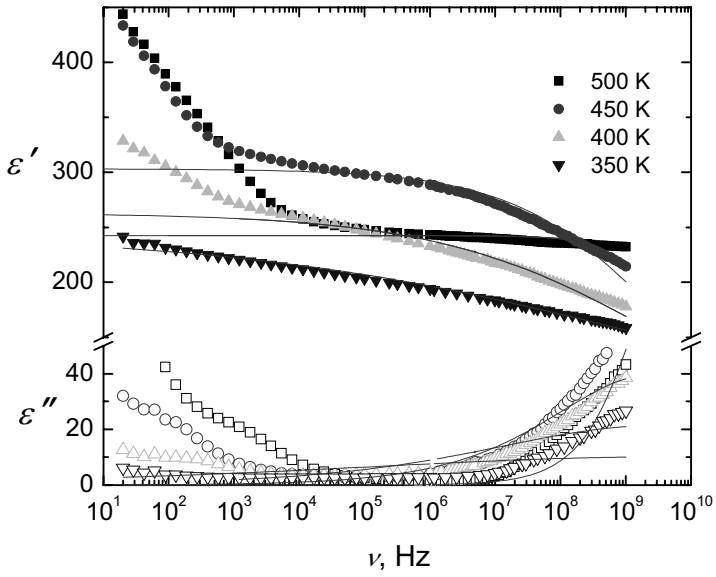

Fig. 5.10. Frequency dependence of the real and imaginary parts of the dielectric permittivity of 0.5BBT-0.5SBT measured in different temperatures.

x = 0.75

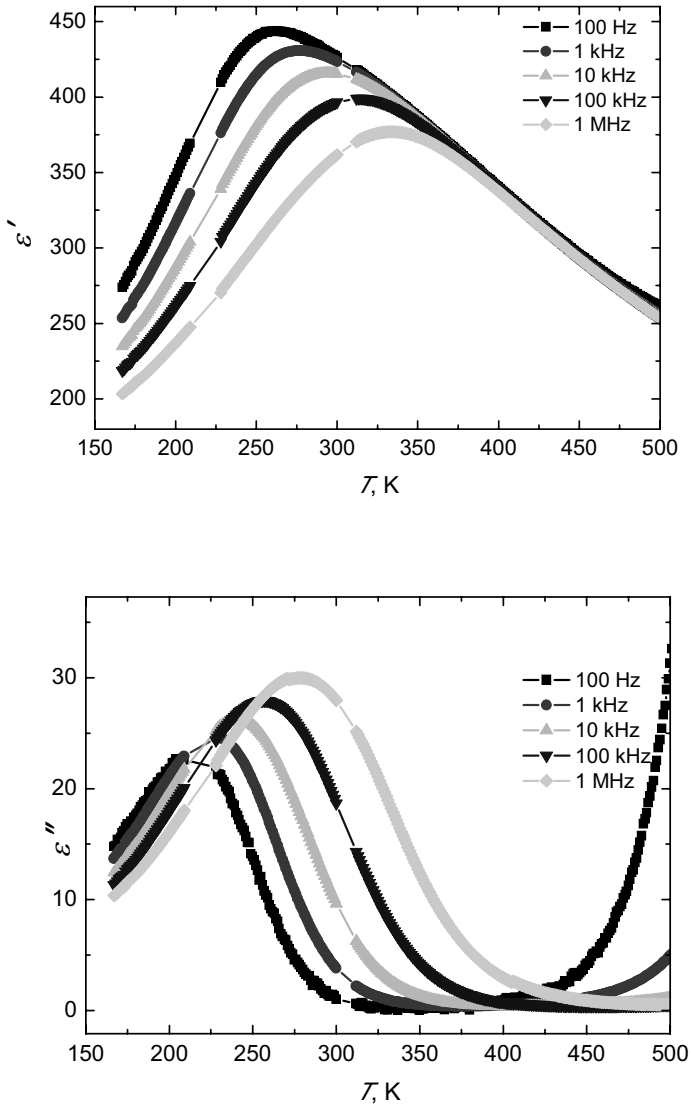

Fig. 5.11. Temperature dependence of the real (a) and imaginary (b) parts of the dielectric permittivity of 0.75BBT-0.25SBT ceramics, measured in different frequencies.

The results of xBBT-(1-x)SBT with x = 0.25, 0.5, 0.75 and 1 confirm the crossover from ferroelectric to relaxor state with decrease of x, although introducing behaviour similar to dipolar glasses.

For BBT (x = 1), the distribution of relaxation times shows complicated nature of the dynamics of this relaxor. We can distinguish at least two different components with different behaviour – most probably we can guess that we observe contributions to the dielectric permittivity originating from the spherical glassy matrix and the ferroelectric clusters. Also this two component behaviour can be related to breathing and flipping motions of the polar nanoregions in the relaxor. These clusters (polar nanoregions) are growing in size and making noticeable influence to the dielectric permittivity of BBT as indicated by asymmetrical broadening of the distribution of relaxation times. As we can see from the distribution function, there are at least two different kinds of polar clusters. Dielectric dispersion in BBT ceramics is much more complicated, due to the broad distribution of the relaxation times even at high temperatures, indicating the influence of polar nanoregions in the whole investigated temperature range.

6. DIELECTRIC AND PFM STUDIES OF $BaBi_2Nb_2O_9$ CERAMICS

The results of this chapter are published in [P1, P3, P6, P8] and were presented in [C1, C6, C15, C19, C21, C23, C30-C34] scientific conferences.

Ba-based ferroelectric ceramics with Bi-layered structure $Ba_xSr_{1-x}Bi_2Nb_2O_9$ ceramics were prepared by mixed oxide route using $SrCO_3$/$BaCO_3$, Bi_2O_3 and Nb_2O_5 as starting reagents. The mixtures of the desired amounts of oxides were milled with planetary ball mill, calcined at 950 ºC for 2 hours, uniaxially pressed at 190 MPa and sintered at temperatures varied in range 1000 – 1250 ºC.

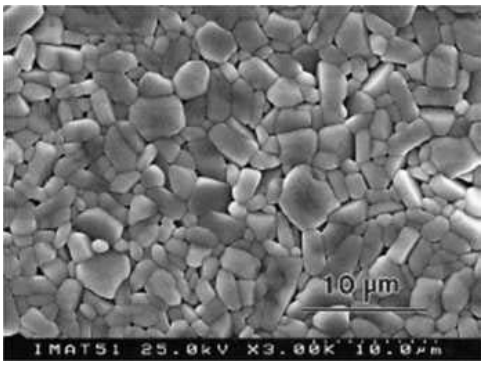

Fig. 6.1. SEM microstructure of $BaBi_2Nb_2O_9$ ceramics sintered at 1100 ºC.

Full substitution of Sr^{2+} with larger Ba^{2+} ions lowers the temperature of the phase transition and the transition becomes broad and dispersive, showing relaxor character. This opens perspective of applications in wide temperature range with still remaining good dielectric and ferroelectric properties.

The real (ε') and imaginary (ε'') parts of dielectric permittivity were measured in temperature interval of 200 – 500 K on cooling at different frequencies (Fig. 6.2). The real part of the dielectric permittivity ε' is strongly dispersive and shifts to higher temperatures with the increase of the frequency. At the lowest

frequency maximum value of 560 of the real part of dielectric permittivity was observed. At high temperatures and low frequencies conductivity contribution was observed, but it was not the aim of the present work. In this paper we will concentrate on the dielectric dispersion.

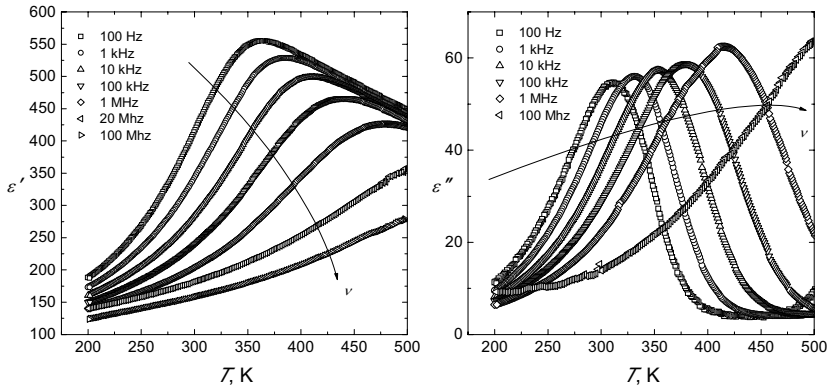

Fig. 6.2. Temperature dependences of the real and imaginary parts of the dielectric permittivity of BBN, measured in different frequencies.

It is comparable with other Ba-based ferroelectrics with Bi-layered structure as BBT but significantly less than for lead containing relaxors as PMN or PLZT. The maximum of the imaginary part of the dielectric permittivity grows with the increase of frequency and shifts to higher temperatures. These temperature dependences are similar to relaxors but are not typical. For relaxors ε'' typically remains nearly constant till the lowest temperatures. As it is typical for dipolar glasses, the maximum of the imaginary part of dielectric permittivity shift to higher temperatures with frequency increasing. Such behaviour is not typical for relaxors. This is also confirmed by frequency dependences of the real and imaginary parts of dielectric permittivity. Frequency dependences of the real and imaginary parts of dielectric permittivity are presented in Fig. 6.3. It should be mentioned, that maxima of the imaginary part of dielectric permittivity shifts much stronger to higher

temperatures with increasing frequency as in lead containing relaxors, such as PLZT.

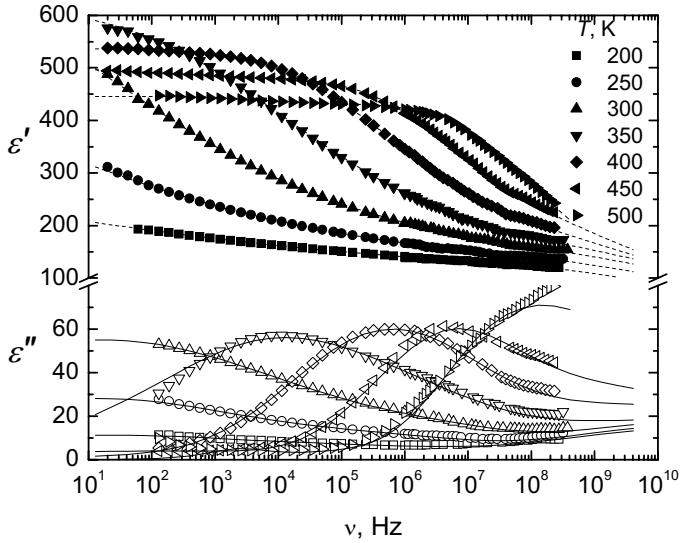

Fig. 6.3. Frequency dependences of the real and imaginary parts of the dielectric permittivity measured in different temperatures.

The dielectric dispersion clearly appears at low temperatures and extends to the microwave region. A less pronounced dispersion of the dielectric permittivity can be seen even at low temperatures. In contrast to the classical relaxors, this dispersion region is temperature dependent and shifts to the lower frequency region with decreasing temperature and we do not observe flat dependence of the imaginary part of the dielectric permittivity, but the real part of dielectric permittivity at low temperatures behaves nearly linearly as it should be for relaxors. At low temperatures we can see appearing second maximum in the frequency dependence of the imaginary part of dielectric permittivity. Low

frequency maximum most probably is related to polar nanoregions dynamics, and a high frequency maximum is caused by nonpolar matrix of ceramics.

We have used usual Cole – Cole model (Eq. 5.1) to obtain dispersion parameters.

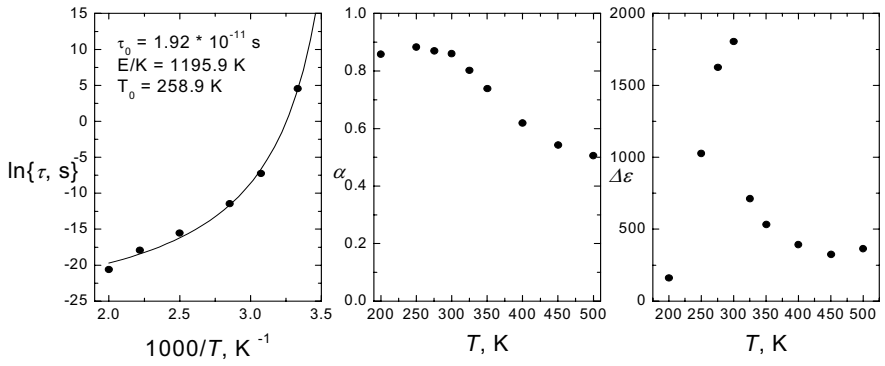

Fig. 6.4. Cole – Cole fit parameters $\Delta\varepsilon$, α, τ.

Calculated Cole-Cole dielectric dispersion parameters are presented in the Fig. 6.4. The parameter of the distribution of relaxation times α has high values in the whole temperature range. At high temperatures it decreases only till 0.5. This means that the distribution of the relaxation times is extremely broad in the whole temperature range.

The mean Cole-Cole relaxation time of present ceramics diverges with temperature according to Vogel-Fulcher law (Eq. 5.2).

The Vogel-Fulcher law parameters are: $\tau_0 = 1.92 \cdot 10^{-11}$ s, $T_0 = 259$ K, $E/k_b = 1196$ K.

However Cole – Cole equation describes symmetrical form of dispersion and can be applied reliably only in such cases. But for BBT ceramics we can see the second process appear in high frequencies (Fig. 6.3). So the original program was used to perform the direct calculation of the relaxation time

distribution function $f(\tau)$ from the frequency dependence of the complex dielectric permittivity at fixed temperatures according to superposition of Debye-like processes (for details, see Chapter 3).

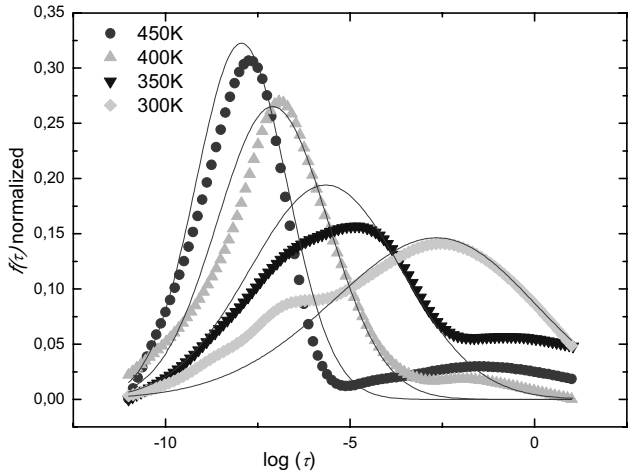

Fig. 6.5 Relaxation time distribution function *f(t)*(normalized) of BBN ceramics at different temperatures.

The real distribution function of the relaxation times $f(\tau)$ was calculated (Fig. 6.5). Even at high temperatures we can clearly see two processes, what is completely different from classic relaxors. High-frequency maximum stays nearly stable, but the most interesting part is the low frequency range. We observe maximum even at high temperatures and this maximum shifts to longer relaxation times with temperature decreasing. This effect can be caused by presence of polar nanoregions and their significant contribution to the dielectric permittivity even at high temperatures. This can mean that Burns temperature for this ceramics is very high, and polar nanoregions are present in the whole investigated temperature range. We consider a polar nanoregion as a dipole moving in an asymmetric double-well potential. The movement consists of fast oscillations in one of the minima with occasional thermally activated

jumps between the minima. Here we neglect quantum tunneling, which is negligible for polar nanoregions. The oscillation frequency is ν_0. The jump probability is governed by the Boltzmann probability of overcoming the potential barrier between the minima. An ensemble of similar relaxations has a relaxational dielectric response at lower frequencies. It was shown that the relaxation time of such system is [42]:

$$\tau = \tau_0 \frac{\exp(E_b / k(T - T_0))}{2\cosh(A / 2kT)}, \qquad (6.1)$$

where $\tau_0 = 1/2\pi\nu_\infty$, T_0 is the Vogel–Fulcher temperature.

We further consider that the dipoles are not similar, but instead have the asymmetry A and the potential barrier E_b randomly distributed according to the Gaussian law around their mean values A_0 and E_{b0}:

$$w(E_b) = \frac{1}{\sqrt{2\pi}\sigma_E} \exp\left(- \frac{(E_b - E_{b0})^2}{2\sigma_E^2} \right), \qquad (6.2)$$

$$w(A) = \frac{1}{\sqrt{2\pi}\sigma_A} \exp\left(- \frac{(A - A_0)^2}{2\sigma_A^2} \right), \qquad (6.3)$$

where σ_E, and σ_A are the standard deviations of E_b and A respectively. Obtained results are shown in the Fig.6.6.

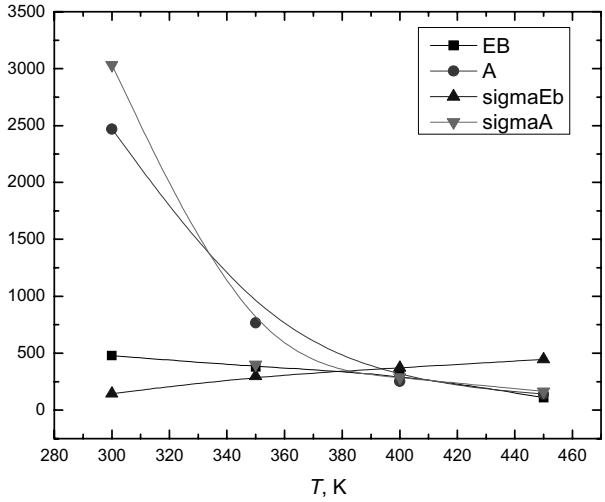

Figure 6.6. Obtained E_b, A, σ_E and σ_A, values at different temperatures.

The conclusion must be made here, that the dipolar glass model is suitable for the relaxors with perovskite structure.

For investigation of the microscopic properties of relaxor ceramics $BaBi_2Nb_2O_9$ (BBN) we have used piezoresponse force microscopy (PFM), which is used to investigate the physical properties at the scale limited only by the diameter of the PFM tip (~10 nm). Detailed microscopic characterizations of the ferroelectric clusters structure were performed. The measure of the short range ordering - correlation length has been directly extracted from the images. The imaging is complemented with local piezoelectric hysteresis acquisition, where the high electric fields can induce local ferroelectric order just under the SFM tip. Polar nanoregions (PNRs) sized about 50 nm were observed in the BBN ceramics. Local ferroelectric hysteresis behaviour was also studied and compared in few different areas of the sample.

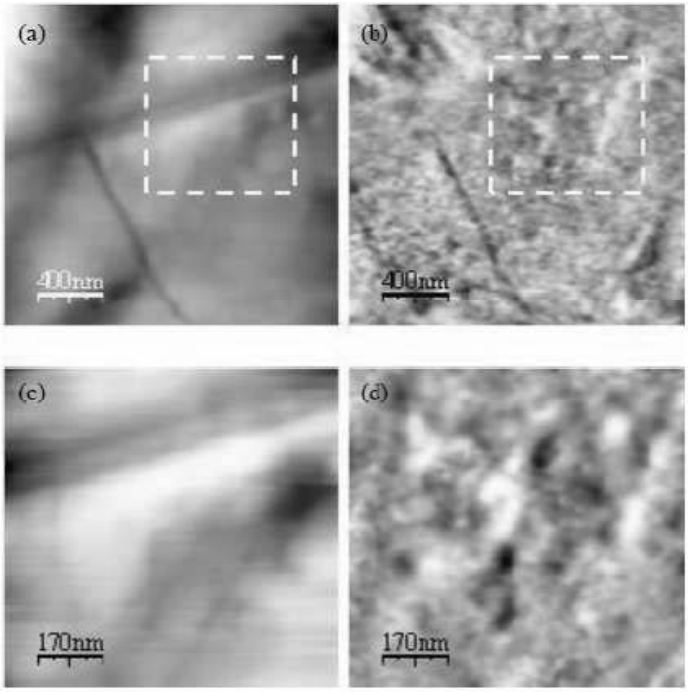

Fig. 6.7. Topography (a, c) and piezoresponse (b, d) images of BBN ceramics.

Our dielectric studies of $BaBi_2Nb_2O_9$ (BBN) in broad frequency range suggested the coexistence of two different phases in this material - the spherical glassy matrix and the ferroelectric clusters. The PNRs are present even at high temperatures and make noticeable influence to the dielectric permittivity of BBN. Dielectric dispersion in BBN ceramics is caused by the presence of two components in the relaxation time distribution even at high temperatures, indicating the influence of polar nanoregions in the whole investigated temperature range.

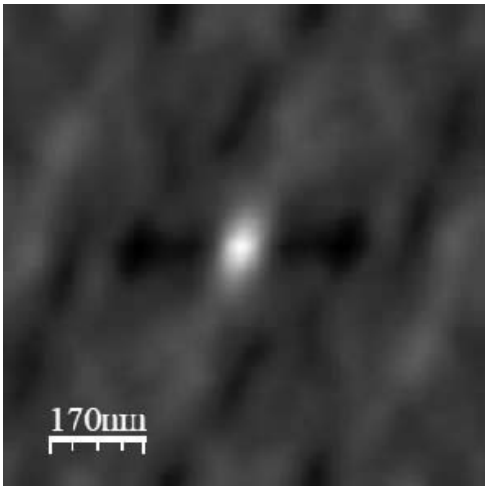

Fig. 6.8. Autocorrelation function image of the PFM contrast from Fig. 6.7 (d).

For the quantitative data treatment, we used a correlation function technique, which has been used for topographic data analysis [79]. Indeed, the value of the signal (contrast) D taken from the piezoresponse image is proportional to the local polarization value. So, its autocorrelation function:

$$C(r_1, r_2) = \sum_{x,y} D(x,y)D(x + r_1, y + r_2) \quad (6.6)$$

is equivalent to polarization-polarization correlation function. The autocorrelation function was used for the estimation of the average size of the nanoregions. The behaviour of the average curve all in-plane directions autocorrelation function was fitted with the formula:

$$C(R) \propto \exp\left(-\left(\frac{R}{R_C}\right)\right)^{2-\alpha} \quad (6.7)$$

where R is radius, R_c - correlation length, a - parameter (in our case $a \approx 0.95 \pm 0.01$) [80].

Even though the freezing occurs below room temperature, the conditions on the surface and strong electric field developed due to the sharp PFM tip may be favorable for the formation of stable ferroelectric state on the surface. In

order to prove this, we applied consecutive voltage pulses and measured the piezoelectric response as a function of the voltage piezoelectric hysteresis loops. We positioned the tip in the center of as-grown nanoregion and swept the voltage in the range −60 V<*V*<+60 V. The results are shown in Fig. 6.9.

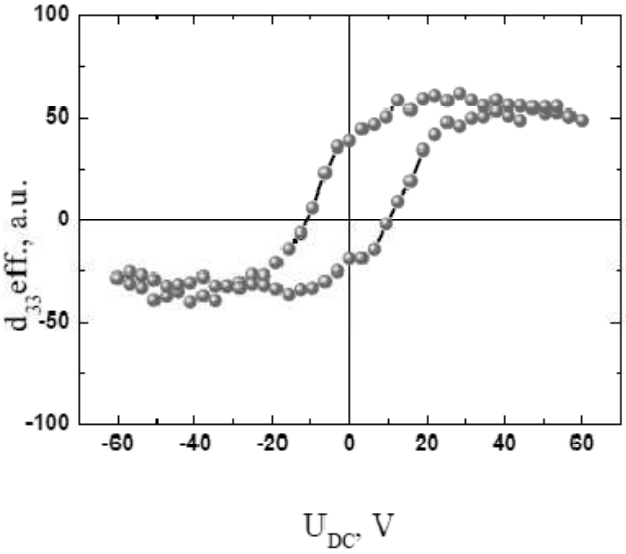

Fig. 6.9. Local piezoresponse hysteresis loop of BBN ceramics

The local piezoelectric coefficient followed normal hysteresis behaviour characteristic of ferroelectric phase with the coercive voltage of about 8–10 V.

After the application of a dc bias, we observed a normal micron-sized ferroelectric domain (Fig. 6.10 a) that was stable and could be still observed ~1 and 2 h after the application of a dc bias field (Fig. 6.10 b,c).

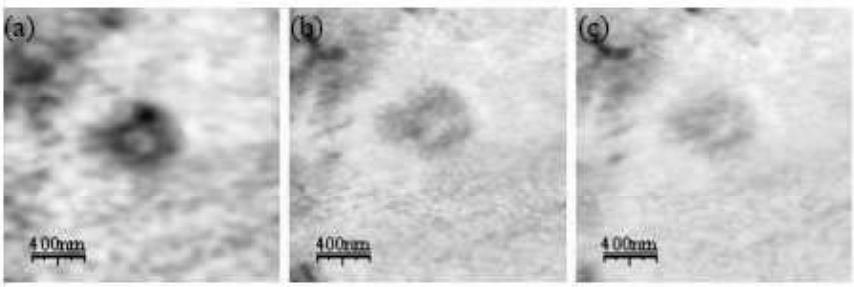

Fig. 6.10. Piezoresponse image (a) just after the application of a bias field, and piezoresponse image relaxation during 1 h (b) and 2 hours (c).

Still open question is the relation of the relaxation time distribution with the distribution of the PNRs sizes.

The conclusions on investigation of BBN ceramics are following:

1. Polar nanoregions have been observed.
2. Dielectric dispersion has features of dipolar glasses
3. The model of dipolar glass double-well potential is suitable for the relaxors with Aurivilius structure.

CONCLUSIONS

1. The (1-x)$BaTiO_3$-x$La(Mg_{1/2}Ti_{1/2}O_3)$ compositions with x = 0.025 and x = 0.05 show ferroelectric and nearly relaxor properties. In this composition we have bridging materials between ferroelectrics and relaxors.
2. Strontium substitution by barium in $Ba_{1-x}Sr_xBi_2Ta_2O_9$ solid solutions induces extremely broad frequency dispersion of the temperature dependence of the dielectric permittivity which is not typical for relaxors or dipolar glasses.
3. The distribution of relaxation times of $BaBi_2Nb_2O_9$ shows the existence of at least two-component behaviour – the spherical glassy matrix and the ferroelectric clusters.

REFERENCES

[1] J. Valasek, Phys. Rev. **17**, 475 (1921).
[2] Official Journal Of The European Union **L 17**, 19-23 (2003).
[3] D. Viehland, S. Jang, L. Cross, and M. Wuttig, Physical Review B **46**, 8003-8006 (1992).
[4] E. Colla, E. Koroleva, N. Okuneva, and S. Vakhrushev, Journal of Physics-Condensed Matter **4**, 3671-3677 (1992).
[5] A. Bokov, Y. Bing, W. Chen, Z. Ye, S. Bogatina, I. Raevski, S. Raevskaya, and E. Sahkar, Physical Review B **68**, (2003).
[6] O. Bidault, C. Perrin, C. Caranoni, and N. Menguy, Journal of Applied Physics **90**, 4115-4121 (2001).
[7] S. Kamba, V. Porokhonskyy, A. Pashkin, V. Bovtun, J. Petzelt, J. Nino, S. Trolier-McKinstry, M. Lanagan, and C. Randall, Physical Review B **66**, (2002).
[8] Y. Wang, S. Bharadwaja, A. Tagantsev, and N. Setter, Journal of the European Ceramic Society **25**, 2521-2525 (2005).
[9] S. Huang, C. Feng, L. Chen, and Q. Wang, Journal of the American Ceramic Society **89**, 328-331 (2006).
[10] S. Saha and T. Sinha, Physical Review B **65**, (2002).
[11] J. Dellis, I. Raevsky, S. Raevskaya, and L. Reznitchenko, Ferroelectrics **318**, 169-177 (2005).
[12] A. Khodorov and A. Tsotsorin, Ferroelectrics **299**, 121-131 (2004).
[13] D. Viehland, S. Jang, E. Cross, and M. Wuttig, Philosophical Magazine a-Physics of Condensed Matter Structure Defects **64**, 835-849 (1991).
[14] J. Malecki and B. Hilczer, Ferroelectric Polymers and Ceramic-Polymer Composites **92-93**, 181-215 (1994).
[15] S. Seo, K. Noh, and S. Kwun, Journal of the Korean Physical Society **35**, 496-499 (1999).
[16] W. Kleemann and R. Lindner, Ferroelectrics **199**, 1-10 (1997).
[17] E. Buixaderas, M. Savinov, M. Kempa, S. Veljko, S. Kamba, J. Petzelt, R. Pankrath, and S. Kapphan, Journal of Physics-Condensed Matter **17**, 653-666 (2005).
[18] S. Park and T. Shrout, Journal of Applied Physics **82**, 1804-1811 (1997).
[19] B. Noheda, Current Opinion in Solid State & Materials Science **6**, 9-9 (2002).
[20] H. Fu and R. E. Cohen, Nature **403**, 281-283 (2000).
[21] S. Kamba, V. Bovtun, J. Petzelt, I. Rychetsky, R. Mizaras, A. Brilingas, J. Banys, J. Grigas, and M. Kosec, Journal of Physics-Condensed Matter **12**, 497-519 (2000).
[22] V. Bovtun, J. Petzelt, V. Porokhonskyy, S. Kamba, and Y. Yakimenko, Journal of the European Ceramic Society **21**, 1307-1311 (2001).
[23] J. Macutkevic, S. Lapinskas, J. Grigas, A. Brilingas, J. Banys, R. Grigalaitis, K. Meskonis, K. Bormanis, A. Sternberg, and V. Zauls, Journal of the European Ceramic Society **25**, 2515-2519 (2005).
[24] M. E. Lines and A. M. (. M.). Glass, *Principles and Applications of Ferroelectrics and Related Materials* (Clarendon Press, Oxford [Eng.] :, 1977).
[25] L. E. Cross, Ferroelectrics **76**, 241 (1987).
[26] G. Burns, Phys. Rev. B **13**, 215 (1976).
[27] R. B. Griffiths, Phys. Rev. Lett. **23**, 17 (1969).
[28] C. Binek and W. Kleemann, Phys. Rev. B **51**, 12888 (1995).

[29] V. Westphal, W. Kleemann, and M. D. Glinchuk, Phys. Rev. Lett. **68**, 847 (1992).
[30] H. Vogel, Phys. Z. **22**, 645 (1921).
[31] G. S. Fulcher, Journal of the American Ceramic Society **8**, 339-355 (1925).
[32] S. B. Vakhrushev, B. E. Kvyatkovsky, A. A. Naberezhnov, N. M. Okuneva, and B. P. Toperverg, Ferroelectrics **90**, 173 (1989).
[33] G. A. Samara, in (Academic Press, 2001), pp. 239-458.
[34] K. Binder and A. P. Young, Rev. Mod. Phys. **58**, 801 (1986).
[35] E. Courtens, Phys. Rev. Lett. **52**, 69 (1984).
[36] Y. Imry and S. Ma, Phys. Rev. Lett. **35**, 1399 (1975).
[37] D. Belanger and A. Young, Journal of Magnetism and Magnetic Materials **100**, 272-291 (1991).
[38] D. S. Fisher, Phys. Rev. Lett. **56**, 416 (1986).
[39] G. Burns, Phase Transitions: A Multinational Journal **5**, 261 (1985).
[40] D. Sherrington and S. Kirkpatrick, Phys. Rev. Lett. **35**, 1792 (1975).
[41] D. Viehland, S. J. Jang, L. E. Cross, and M. Wuttig, Phys. Rev. B **46**, 8003 (1992).
[42] R. Blinc, J. Dolinšek, A. Gregorovič, B. Zalar, C. Filipič, Z. Kutnjak, A. Levstik, and R. Pirc, Phys. Rev. Lett. **83**, 424 (1999).
[43] W. Cochran, Advances in Physics **9**, 387 (1960).
[44] J. Harada, J. D. Axe, and G. Shirane, Phys. Rev. B **4**, 155 (1971).
[45] B. Zalar, V. V. Laguta, and R. Blinc, Phys. Rev. Lett. **90**, 037601 (2003).
[46] T. Mitsui and W. B. Westphal, Phys. Rev. **124**, 1354 (1961).
[47] D. Hennings and G. Rosenstein, Journal of the American Ceramic Society **67**, 249-254 (1984).
[48] S. Swartz, Ieee Transactions on Electrical Insulation **25**, 935-987 (1990).
[49] W. Buessem, L. Cross, and A. Goswami, Journal of the American Ceramic Society **75**, 2923-2926 (1992).
[50] G. Arlt, D. Hennings, and G. de With, J. Appl. Phys. **58**, 1619 (1985).
[51] F. Bahri, A. Simon, H. Khemakhem, and J. Ravez, Physica Status Solidi a-Applied Research **184**, 459-464 (2001).
[52] A. Simon, J. Ravez, and M. Maglione, Journal of Physics-Condensed Matter **16**, 963-970 (2004).
[53] N. Salak, P. Seabra, and V. Ferreira, Ferroelectrics **318**, 185-192 (2005).
[54] W. Xiaoyong, F. Yujun, and Y. Xi, Appl. Phys. Lett. **83**, 2031 (2003).
[55] S. G. Lu, Z. K. Xu, and H. Chen, Appl. Phys. Lett. **85**, 5319 (2004).
[56] L. Geske, H. Beige, H. Abicht, and V. Mueller, Ferroelectrics **314**, 97 (2005).
[57] V. Shvartsman, W. Kleemann, J. Dec, Z. Xu, and S. Lu, Journal of Applied Physics **99**, (2006).
[58] V. Mueller, H. Beige, and H. Abicht, Appl. Phys. Lett. **84**, 1341 (2004).
[59] K. Oh, K. Uchino, and L. Cross, Journal of the American Ceramic Society **77**, 2809-2816 (1994).
[60] G. A. Smolenskii and V. A. Isupov, Zh. Tekh. Fiz. **24**, 1375 (1954).
[61] B. Aurivilius, Ark. Kemi **1**, 463 (1949).
[62] L. E. Cross, in *Ferroelectric Ceramics-Tutorial Reviews, Theory, Processing and Applications*, 1st ed. (Birkhauser Verlag, Basel, 1993).
[63] E. C. Subbarao, Journal of Physics and Chemistry of Solids **23**, 665-676 (1962).
[64] S. Swartz, W. A. Schulze, and J. V. Biggers, Ferroelectrics **38**, 765 (1981).
[65] Y. Shimakawa, Y. Kubo, Y. Nakagawa, S. Goto, T. Kamiyama, H. Asano, and F. Izumi, Physical Review B **61**, 6559-6564 (2000).

[66] G. A. Smolenskii, V. A. Isupov, and A. I. Agranovskaya, Sov. Phys. Solid State **3**, 651 (1961).
[67] A. Rae, J. Thompson, and R. Withers, Acta Crystallographica Section B-Structural Science **48**, 418-428 (1992).
[68] R. Macquart, B. J. Kennedy, T. Vogt, and C. J. Howard, Phys. Rev. B **66**, 212102 (2002).
[69] M. Avdeev, A. L. Kholkin, M. E. V. Costa, and J. Baptista, Kem **230-232**, 595-598 (2002).
[70] C. A. de Araujo, J. D. Cuchiaro, L. D. McMillan, M. C. Scott, and J. F. Scott, Nature **374**, 627-629 (1995).
[71] J. F. Scott, Ferroelectrics **183**, 51 (1996).
[72] B. H. Park, B. S. Kang, S. D. Bu, T. W. Noh, J. Lee, and W. Jo, Nature **401**, 682-684 (1999).
[73] A. Brandt, *Issledovanie Dielektrikov Na Sverchvysokich Castotach* (Fizmatgiz, Moscow, 1963).
[74] A. Brilingas, R. L. Davidovich, J. Grigas, S. Lapinskas, M. A. Medkov, V. Samulionis, and V. Skritskii, Physica Status Solidi (a) **96**, 101-109 (1986).
[75] J. Grigas, *Microwave Dielectric Spectroscopy of Ferroelectrics and Related Materials* (Gordon and Breach Science Publ., OPA Amsterdam, 1996).
[76] M. P. Seabra and V. M. Ferreira, Materials Research Bulletin **37**, 255-262 (2002).
[77] J. Macutkevic, J. Banys, and A. Matulis, Nonlinear Analysis: Modelling and Control **9**, 75-88 (2004).
[78] M. Maglione, R. Böhmer, A. Loidl, and U. T. Höchli, Phys. Rev. B **40**, 11441 (1989).
[79] V. Shvartsman, A. Kholkin, A. Orlova, D. Kiselev, A. Bogomolov, and A. Sternberg, Applied Physics Letters **86**, (2005).
[80] S. K. Sinha, E. B. Sirota, S. Garoff, and H. B. Stanley, Phys. Rev. B **38**, 2297 (1988).